

**Charles University**

**Faculty of Science**

Study programme: Chemistry

Branch of study: Biophysical chemistry



**Bc. Anastasia Rakhimbekova**

Structure-assisted development of a continuous carboxypeptidase assay

Vývoj substrátů pro kontinuální fluorescenční stanovení karboxypeptidasové aktivity s  
využitím rentgenostrukturní analýzy

Diploma thesis

Supervisor:

RNDr. Cyril Bařinka, Ph.D.

Consultants:

Ing. Zsófia Kutil, PhD, Mgr. Lucia Motlová, Mgr. Jana Mikešová

Prague, 2021

## **Prohlášení**

Prohlašuji, že jsem závěrečnou práci zpracovala samostatně a že jsem uvedla všechny použité informační zdroje a literaturu. Tato práce ani její podstatná část nebyla předložena k získání jiného nebo stejného akademického titulu.

V Praze dne 21.06.2021

.....

## **Abstract**

Glutamate carboxypeptidase II (GCPII) is a zinc-dependent carboxypeptidase with high expression levels in prostate carcinoma. As the enzyme represents a validated target for cancer therapy and imaging, the development of new GCPII-specific ligands is still a focus of an active academic and industrial research. However, existing assays to screen inhibitor libraries and determine inhibitor efficacy are suboptimal at best.

This thesis is aimed at the development of small internally quenched probes that could be used for continuous measurement of the GCPII enzymatic activity. These probes are derived from natural GCPII substrates and consist of a fluorophore/quencher pair connected by a GCPII-hydrolysable linker. I first characterized biophysical properties of the probes and then determined kinetic parameters of their hydrolysis by GCPII. The optimized activity assay was then used to determine inhibition constants of several GCPII-specific inhibitors. Finally, complexes between the inactive enzyme and several probes were co-crystallized and one of the complexes refined and analyzed. Our data show that the probes are involved in non-covalent interactions with the same amino acid residues of the enzyme's active site as natural substrates. The developed assay could be optimized for high-throughput screening of small-compound libraries in search of potential GCPII inhibitors.

**Key words:** glutamate carboxypeptidase II, internally quenched fluorescent probes, enzyme kinetics; X-ray crystallography

## **Abstrakt**

Glutamát karboxypeptidasa II (GCPII) je zinek-dependentní karboxypeptidasa s vysokou hladinou exprese u karcinomu prostaty. Vzhledem k tomu, že daný enzym představuje ověřený cíl pro terapii a zobrazování rakoviny, je vývoj nových ligandů specifických pro GCPII stále předmětem aktivního akademického a průmyslového výzkumu. Stávající analýzy pro screening knihoven inhibitorů a stanovení účinnosti inhibitorů nejsou však optimální.

Tato diplomová práce je zaměřena na vývoj malých interně zhášených sond, které by mohly být použity pro kontinuální měření enzymatické aktivity GCPII. Tyto sondy jsou odvozeny z přirozených substrátů GCPII a sestávají z páru fluorofor/zhášeč spojeného GCPII-hydrolyzovatelným linkerem. Nejprve jsem charakterizovala biofyzikální vlastnosti sond a poté stanovila kinetické parametry jejich hydrolýzy GCPII. Optimalizovaná metoda pro stanovení karboxypeptidasové aktivity byla použita pro určení  $IC_{50}$  u několika GCPII-specifických inhibitorů. Nakonec komplexy mezi neaktivním enzymem a uvedenými sondami byly kokrytalizovány, a pro jeden z komplexů byly provedeny upřesnění a analýza struktury. Naše data naznačují, že sondy jsou zapojeny do nekovalentních interakcí se stejnými aminokyselinovými zbytky aktivního místa enzymu jako přirozené substráty. Vyvinutá analýza může být optimalizována pro vysokovýkonný screening knihoven malých sloučenin pro hledání potenciálních inhibitorů GCPII.

**Klíčová slova:** glutamát karboxypeptidasa II, interně zhášené fluorescenční sondy, enzymová kinetika, X-ray krystalografie

## **Acknowledgments**

I would like to express my gratitude to Cyril Bařinka for the opportunity to work in his lab, the opportunity to visit BESSYII, and his guidance during these two years. I also would like to thank Zsófia Kutil for her enormous help with experiments and correction of this thesis, Lucia Motlová for teaching me how to crystallize proteins and to do refinement, Jana Mikešová for introducing me to CLARIOstar, all members of our lab for creating friendly environment and willingness to help. I am grateful to Dr. Jiří Pavlíček and Dr. Jan Stránský for providing their help with data collection and willingness to discuss problems related to protein structure solving, and to Dr. Marat Meleshin for providing us with the substrates. I also thank my family and friends for their support during my student years.

## List of abbreviations

cAMP – cyclic adenosine monophosphate

CCL5 – CC-chemokine ligand 5

cGMP – cyclic guanosine monophosphate

CRISPR – clustered regularly interspaced short palindromic repeats

CT – computed tomography

DFO – desferrioxamine

DMSO – dimethylsulfoxide

DOTA – dodecane tetraacetic acid

DTPA – diethylenetriaminepentaacetic acid

Fab – antigen-binding fragment

FDA – Food and Drug Administration

FOH1 – folate hydrolase 1

GCPII – glutamate carboxypeptidase II

HPLC – high-performance liquid chromatography

HRP – horseradish peroxidase

HTS – high-throughput screening

IC<sub>50</sub> – half maximal inhibitory concentration

IL-6 – interleukin 6

IR – infrared

k<sub>cat</sub> – turnover number

K<sub>m</sub> – Michaelis constant

2MeTG – 2-methyl TokyoGreen

mGluR – metabotropic glutamate receptor

MRI – magnetic resonance imaging

NAAG – N-acetyl-L-aspartyl-L-glutamate

NF-κB – nuclear factor kappa-light-chain-enhancer of activated B cells

OPA – *o*-phthalaldehyde

PABG $\gamma$ G – N-(4-phenylazobenzoyl)-glutamyl- $\gamma$ -glutamic acid

PEG – polyethylene glycol

PET – positron emission tomography

2-PMPA – 2-(phosphonomethyl)pentanedioic acid

PSMA – prostate-specific membrane antigen

QM/MM – quantum mechanics/molecular mechanics

rh – recombinant human

RNAi – RNA interference

scFv – Single-chain variable fragment

SELEX – systematic evolution of ligands by exponential enrichment

SH3 – SRC Homology 3

SPECT – single-photon emission computed tomography

SPION – superparamagnetic iron oxide nanoparticle

TFA – trifluoroacetic acid

TGF- $\beta$  – transforming growth factor  $\beta$

UPLC – ultra performance liquid chromatography

UV – ultraviolet

## Table of contents

<b>1. Introduction</b> .....	1
<b>1.1. Expression and functions of GCPII in human tissues</b> .....	1
<b>1.1.1. Under normal conditions</b> .....	1
<b>1.1.2. Under pathological conditions</b> .....	3
<b>1.1.2.1. Possible role in cancer</b> .....	3
<b>1.1.2.2. GCPII as a prostate cancer biomarker and a therapy target</b> .....	4
<b>1.2. Targeting GCPII – small-molecule inhibitors, antibodies, aptamers</b> .....	5
<b>1.2.1. Monoclonal antibodies</b> .....	5
<b>1.2.2. Aptamers</b> .....	6
<b>1.2.3. Small-molecule inhibitors</b> .....	7
<b>1.2.3.1. Phosphorus-based inhibitors</b> .....	8
<b>1.2.3.2. Thiol-based inhibitors</b> .....	9
<b>1.2.3.3. Urea-based inhibitors</b> .....	10
<b>1.2.3.4. Hydroxamic acid-based inhibitors</b> .....	11
<b>1.3. Structural characteristics of GCPII</b> .....	12
<b>1.3.1. Binding cavity</b> .....	14
<b>1.3.2. Posttranslational modifications</b> .....	17
<b>1.3.3. Quaternary structure</b> .....	18
<b>1.4. Mechanism of catalysis</b> .....	18
<b>1.5. Existing GCPII activity assays</b> .....	20
<b>1.5.1. Radioenzymatic assay</b> .....	20
<b>1.5.2. Fluorescence end-point assay</b> .....	20
<b>1.5.3. HPLC-based assay</b> .....	21
<b>1.5.4. Fluorescence polarization assay</b> .....	21
<b>1.5.5. Amplex Red glutamic acid assay</b> .....	22
<b>1.5.6. Fluorescence continuous assay</b> .....	22
<b>2. Aims</b> .....	23
<b>3. Experimental part</b> .....	24
<b>3.1. Materials</b> .....	24
<b>3.2. Methods</b> .....	26
<b>3.2.1. Fluorescence signal linearity – microplate readout</b> .....	26
<b>3.2.2. Kinetic measurements – microplate readout</b> .....	27
<b>3.2.3. Kinetic measurements – HPLC readout</b> .....	28
<b>3.2.3.1. Method development</b> .....	28



3.2.3.2.	Kinetic measurements .....	29
3.2.4.	GCPII activity assay (measurement of IC <sub>50</sub> of T33D and DCIBzL) .....	30
3.2.5.	Crystallization and data collection.....	30
3.2.6.	Structure determination and refinement.....	31
3.3.	Results .....	32
3.3.1.	Fluorescence signal linearity – microplate readout .....	32
3.3.2.	Kinetic measurements – microplate readout .....	34
3.3.3.	Kinetic measurements – HPLC readout.....	36
3.3.3.1.	Method development .....	36
3.3.3.2.	Kinetic measurements .....	38
3.3.4.	Determination of IC <sub>50</sub> values for T33D and DCIBzL inhibitors .....	39
3.3.5.	Crystallization and data collection.....	39
3.3.6.	Structure determination and refinement.....	41
3.4.	Discussion.....	45
3.5.	Conclusions .....	49
4.	References .....	50

## 1. Introduction

Glutamate carboxypeptidase II (GCPII, E.C. 3.4.17.21), also called (depending on its localization and/or physiological function) prostate-specific membrane antigen, N-acetyl-L-aspartyl-L-glutamate peptidase I, and folate hydrolase 1, is a zinc-dependent membrane resident exopeptidase. It consists of 750 amino acids and has a molecular weight of about 100 kDa<sup>1</sup>. GCPII plays an important role as a biomarker and a target for the treatment of androgen-resistant prostate carcinoma<sup>2</sup>. It is also a promising therapeutic target for numerous neurological diseases, since inhibition of its brain form has neuroprotective effects<sup>3</sup>.

In humans, GCPII is coded by the *FOHI* gene located on the short arm of the 11th chromosome at the 11p11.2 position and composed of 19 exons and 18 introns<sup>4</sup>. Orthologs of the gene exist in a various range of animal species and are not present in plants and yeasts<sup>5</sup>. Rat, mouse, and pig GCPII share more than 90% similarity with human GCPII<sup>6,7,8</sup>. However, GCPII expression profile varies among different species<sup>7,9,10</sup>. In this thesis, only human GCPII and its expression will be discussed.

### 1.1. Expression and functions of GCPII in human tissues

#### 1.1.1. Under normal conditions

GCPII is expressed in the following tissues: brain tissue, prostate epithelium, kidney proximal tubules, and small intestine<sup>2,11-13</sup>. Data about the expression in other tissues are sometimes contradicting, although disagreement between publications possibly arises from the differences in methods used. Lower levels of protein expression were detected in the salivary gland, breast, heart, bladder, colon, liver, ovaries, testis, and other tissues<sup>2,9,14-16</sup>. GCPII physiological function as a peptidase is known only for the nervous system and the small intestine.

In the nervous system, GCPII is expressed on membranes of astrocytes and acts as N-acetyl-L-aspartyl-L-glutamate hydrolase, cleaving NAAG to N-acetyl-L-aspartate and L-glutamate<sup>17</sup>. NAAG is an important widely distributed neurotransmitter of the mammalian nervous system present in millimolar concentrations<sup>18,19</sup>. It is stored in synaptic vesicles of presynaptic axonal terminals<sup>20,21</sup> and is released to the synaptic cleft upon depolarization in a calcium-dependent manner<sup>22-24</sup>. Here, NAAG could act as an agonist of type 3 metabotropic glutamate receptors (mGluR3), located on presynaptic neurons or glia cells, and as an agonist/antagonist of N-methyl-D-aspartate receptors (dependent on their subunit composition and pH)<sup>25,26</sup>. NAAG activation of mGluR3 receptors leads to a decrease in cAMP and cGMP intracellular

concentrations *via* a G-protein coupled pathway<sup>26,27</sup>. In astrocytes, this event stimulates production and secretion of transforming growth factor  $\beta$  (TGF- $\beta$ )<sup>28</sup>, while activation of neuronal mGluR3 leads to the reduction in a release of glutamate, the main excitatory neurotransmitter<sup>29</sup>.

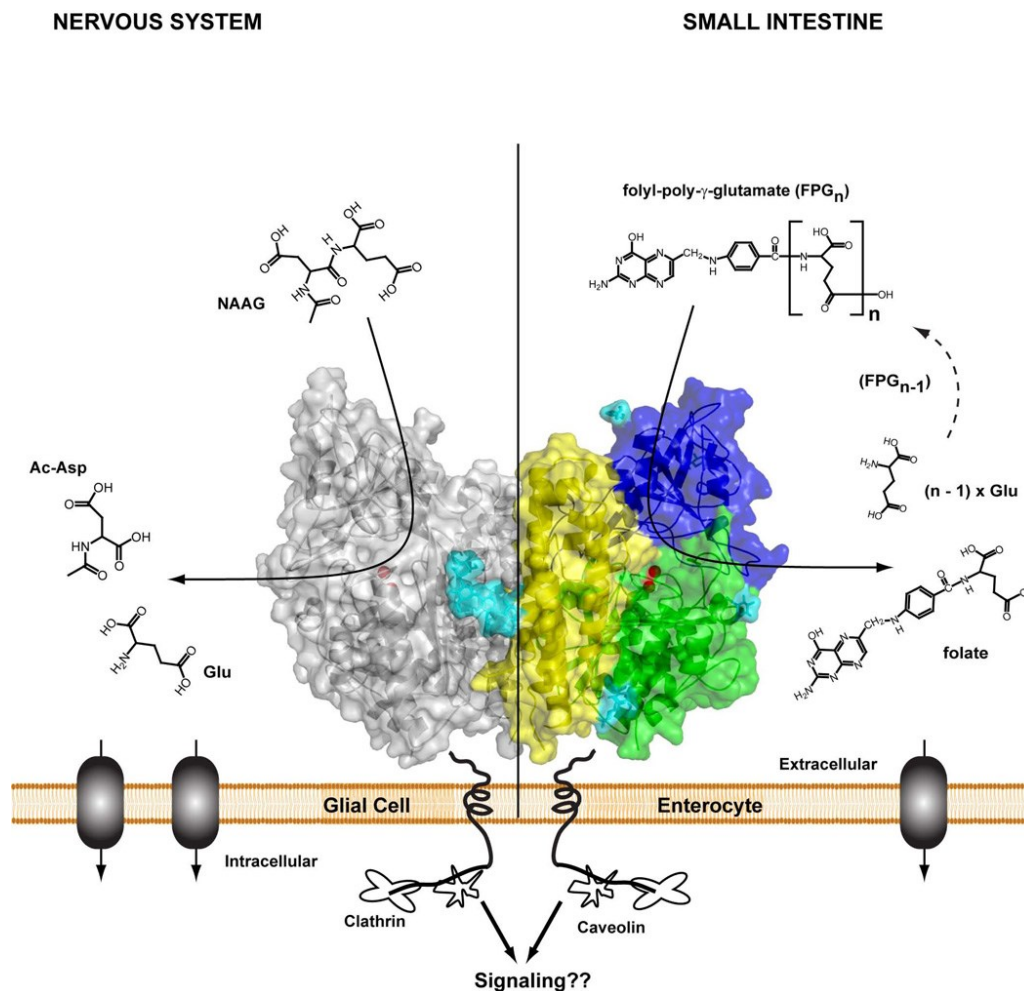


**Figure 1. A human GCPII homodimer resident in a biological membrane**

One monomer is shown in semitransparent surface representation with individual domains of the extracellular part colored green (protease domain), blue (apical domain), and yellow (C-terminal domain); the second monomer is colored gray. N-linked carbohydrates are colored cyan,  $Zn^{2+}$  ions at the active site are shown as red spheres. Left panel – GCPII resident at the plasma membrane of glial cells catabolizes NAAG, leaving N-acetyl-L-aspartate and L-glutamate. Right panel– GCPII at the plasma membrane of enterocytes in the proximal small intestine sequentially hydrolyzes the C-terminal  $\gamma$ -glutamate tail of dietary folates, finally leaving folate with a single glutamate moiety, which can be actively transported into the bloodstream. The figure was reproduced from Barinka, C., Rojas, C., Slusher, B. & Pomper, M. Glutamate Carboxypeptidase II in Diagnosis and Treatment of Neurologic Disorders and Prostate Cancer. *Curr. Med. Chem.* **19**, 856–870 (2012)<sup>39</sup>.

Both TGF- $\beta$  secretion and glutamate release suppression are neuroprotective<sup>28,30</sup>. Inhibition of GCPII could bring neuroprotective effect, since 1) uncleaved NAAG could activate mGluR3 receptors 2) additional glutamate is not generated upon NAAG cleavage by GCPII<sup>3,26</sup>.

The physiological role of GCPII enzymatic activity at the proximal small intestine brush border is also well known. GCPII expressed at the enterocyte membranes cleaves C-terminal glutamate moieties from dietary poly- $\gamma$ -glutamylated folates<sup>31</sup>, at the end leaving folate that possess only one glutamate moiety. Unlike polyglutamated components, folate could be transferred through the intestine wall into the blood stream<sup>32</sup>. Folate is an important vitamin required for the synthesis of nucleotides and methionine. Folate deficiency is associated with megaloblastic anemia<sup>33</sup>, neural tube defects<sup>34</sup>, cardiovascular diseases<sup>35</sup>, and colon cancer risk<sup>36</sup>. In 2000, Devlin et al. stated that His475Tyr polymorphism in GCPII is connected with 53% less effective folate hydrolysis. They found it to lead to impaired folate intestinal absorption, which results in low folate levels in blood<sup>37</sup>. However, the study by Navratil et al. finds GCPIIHis475Tyr enzymatic activity and structure to be similar to wild type GCPII, although the mutation could be influencing folate metabolism by other means (such as changes of GCPII trafficking, expression, or interactions with potential signaling partners)<sup>38</sup>. Studies of further effects of that polymorphism provided inconclusive and contradicting data<sup>39-41</sup>.

### **1.1.2. Under pathological conditions**

GCPII expression was detected in androgen-resistant prostate cancer, prostate cancer metastases (bone and lymph node), schwannoma, malignancies in kidney, bladder, liver, lung, breast, colon, solid tumor neovasculature, and other pathological tissues<sup>2,13-15,42-46</sup>. GCPII is also expressed in the neovasculature of benign reparative tissues such as the endometrium, granulation tissue, and keloid scars<sup>47</sup>. The highest expression level in pathological tissues is connected with androgen-resistant prostate cancer, and, although GCPII is not exclusively located in prostate tissue, it remains a sensitive and specific marker for prostate adenocarcinoma<sup>2</sup> (will be further discussed in the chapter 1.1.2.2).

#### **1.1.2.1. Possible role in cancer**

GCPII expression is upregulated in malignant tissues and its extend correlates with tumor progression, thus, GCPII is a potential contributor to carcinogenesis<sup>2</sup>. However, the precise role of GCPII in this process is not known. Two ways of contribution are possible – by the proteolytic activity or by nonenzymatic receptor-like function<sup>48-50</sup>.

In cancer cells, GCPII enzymatic activity is higher in comparison with normal or benign neoplastic tissues<sup>51</sup>. Under physiological conditions, GCPII was found to provide a growth advantage *via* its folate hydrolase activity<sup>48</sup>. By folyl-poly- $\gamma$ -glutamate hydrolysis, GCPII generates folate and free glutamate. Folate could be transferred into cells. It was also proposed that GCPII could increase an uptake of already present folate behaving as a transporter<sup>52</sup>. Free glutamate from folyl-poly- $\gamma$ -glutamate cleavage or cleavage of other substrates (for example, NAAG, which is more abundant in high-grade cancers<sup>53</sup>) activates group 1 metabotropic glutamate receptors (mGluRI), subsequently activating phosphoinositide 3-kinase and by that facilitating oncogenic signaling<sup>54</sup>. Enzymatic activity of GCPII was also found to be necessary for endothelial cell invasion *in vitro*<sup>49</sup>. Conway et al. proposed that the laminin-derived LQE peptide can serve as a GCPII substrate<sup>55</sup>. The product of its cleavage, LQ, promotes integrin activation and phosphorylation of focal adhesion kinase, by that contributing to tumor angiogenesis.

Another impact of GCPII is related to its nonenzymatic role in signaling. It activates RAS-RAC1-MAPK pathway leading to activation of NF- $\kappa$ B transcription factor and increase in expression of IL-6 and CCL5 genes, thus enhancing cancer cell proliferation and promoting apoptosis resistance<sup>50</sup>. However, a binding partner of GCPII has not been identified yet. GCPII was also found to be associated with the anaphase-promoting complex in prostate carcinoma cells, leading to premature mitotic exit and aneuploidy<sup>56</sup>.

#### **1.1.2.2. GCPII as a prostate cancer biomarker and a therapy target**

In normal tissue, mainly N-truncated form of GCPII called PSM<sup>7</sup>, which lacks transmembrane and intracellular domains (amino acids 1-59), is found in the cytosol. That form is N-glycosylated, enzymatically active, and, most probably, does not arise from the alternative splicing, but is a result of posttranslational cleavage<sup>57</sup>. In prostate carcinoma, membrane-resident full-length GCPII prevails, with expression much higher than in normal or benign prostate tissue and expression levels increasing with the Gleason score<sup>58</sup>. GCPII expression inversely correlates with a degree of tumor differentiation, with greater expression levels being in poorly differentiated, aggressive tumors<sup>59</sup>.

Because of all above mentioned and high specificity of GCPII to a prostate carcinoma (95%)<sup>2</sup>, GCPII is viewed as an important diagnostic biomarker. Another area where GCPII imaging potential could be implemented is solid tumor neovasculature imaging, since the vasculature of corresponding healthy tissues does not express GCPII<sup>60</sup>. However, Gordon et al.

described GCPII expression in the neovasculature of benign reparative tissues<sup>47</sup>. For GCPII molecular imaging, PET and SPECT remain the most used techniques.

GCPII could be considered a therapeutic and imaging target in the case of prostate cancer, taking into account its role in proliferation (described in the chapter 1.1.2.1) and high expression levels. GCPII is a promising therapeutic target in the case of neurological pathologies connected with glutamate excitotoxicity, since its inhibition leads to an increase in NAAG concentration and a decrease of glutamate concentration, leading to a neuroprotective effect. GCPII potential in therapy has been shown in preclinical models of neurological diseases including Alzheimer dementia<sup>61</sup>, traumatic brain injury<sup>62</sup>, ischemia<sup>63</sup>, amyotrophic lateral sclerosis<sup>64</sup>, multiple sclerosis<sup>65</sup>, inflammatory pain<sup>66</sup>, neuropathic pain<sup>67</sup>, peripheral neuropathy<sup>68</sup>, epilepsy<sup>69</sup>, and schizophrenia<sup>70</sup>.

## **1.2. Targeting GCPII – small-molecule inhibitors, antibodies, aptamers**

For GCPII targeting, three main groups of ligands are investigated – antibodies, aptamers, and small-molecule inhibitors<sup>71</sup>. To enable imaging by PET or SPECT those ligands should be labeled with a  $\beta^+$  radioisotope. Another option for imaging is conjugation with an IR-fluorescent dye as described by Chen et al<sup>72</sup>. For the therapy, three main strategies are used – developing conjugates of a GCPII-targeting moiety with a cytotoxic moiety (radioisotope or toxin), conjugates delivering RNAi/therapeutic genes, or immunotherapeutics that trigger an immune response by interaction with GCPII, leading to death of GCPII-expressing cells<sup>73</sup>.

### **1.2.1. Monoclonal antibodies**

Monoclonal antibodies are used for molecular imaging and therapy. For the first time, prostatic GCPII was discovered with the use of the 7E11-C5 antibody<sup>74</sup>. Its radiolabeled derivate, the 7E11/CYT-356 antibody, marketed as ProstaScint<sup>TM</sup> by Cytogen Corporation, was the first agent approved by the FDA for prostate carcinoma imaging in humans<sup>75,76</sup>. This is an originally murine antibody conjugated with pentetide chelating <sup>111</sup>In. It recognizes six amino acid residues in the intracellular part of GCPII<sup>77</sup>. ProstaScint<sup>TM</sup> staging of the primary prostate cancer has 68% accuracy, 62% sensitivity, and 72% specificity, all the parameters being acceptable but relatively low<sup>75</sup>. The main problem in imaging with ProstaScint<sup>TM</sup> arises from the nonspecific tissue uptake that creates high background signal<sup>78</sup>. Another problem is long circulation times, however, this issue is typical for antibodies. Intracellular localization of the epitope makes only GCPII from necrotic/apoptotic cells available for targeting, thus limiting

antibody detection capacity. ProstaScint™ fails to reliably detect bone metastases<sup>79</sup>, and ProstaScint™ analog labeled with <sup>90</sup>Y was found to be almost ineffective in therapy<sup>80</sup>.

Antibodies recognizing epitope in the extracellular domain of GCPII were also prepared, being the most clinically advanced<sup>79</sup>. The humanized form of mouse J591 has been engineered to lower its immunogenicity<sup>81</sup>. J591 conjugated with DTPA/DOTA/DFO chelating agents can be labeled with <sup>111</sup>In, <sup>89</sup>Zr, <sup>64</sup>Cu for imaging and <sup>90</sup>Y, <sup>177</sup>Lu, <sup>131</sup>I, <sup>213</sup>Bi, <sup>225</sup>Ac for therapy<sup>82-88</sup>. Similarly to ProstaScint™, J591 conjugates are taken by non-target tissues, however, they display a higher tumor/background ratio and allow detection of bone lesions as well<sup>84,89</sup>. A conjugate of J591 with the near-IR fluorophore was also developed for imaging<sup>90</sup>. J591 conjugates with the ricin A chain, melittin-like peptide 101, and maytansinoid 1 were studied *in vitro* and using mouse xenograft models<sup>91-93</sup>. The latter conjugate entered clinical trials<sup>94</sup>.

Monoclonal antibodies 3/F11, 3/E7, and 3/A12 bind to epitopes in the extracellular domain of GCPII<sup>95</sup>. Conjugates of each of them with DOTA labeled with <sup>64</sup>Cu show specific uptake and high tumor/background ratio<sup>96</sup>. Another monoclonal antibody 5D3 not only shows specific uptake *in vivo* in mice models but also has a 10-fold higher affinity towards GCPII than J591<sup>97</sup>.

To improve pharmacokinetic properties and targeting of the agent, small antibody fragments and synthetic immunological constructs maintaining the epitope binding part are engineered. Such agents include single domain antibody fragments (nanobodies), Fab and single-chain variable fragments, diabodies (scFv dimers), and minibodies (scFv-fusion proteins)<sup>98-102</sup>.

### 1.2.2. Aptamers

Another strategy for improving pharmacokinetics comparing with intact antibodies is the development of RNA and DNA aptamers as targeting agents. RNA or DNA aptamers are short sequences of oligonucleotides, which bind to their targets with high affinity and specificity<sup>103</sup>. They are derived from randomized aptamer libraries by the process called SELEX (systematic evolution of ligands by exponential enrichment)<sup>104</sup>. Unlike antibodies, aptamers tend to have shorter circulation times and are less immunogenic, thus being preferable targeting agents<sup>105,106</sup>. Their small size allows better permeability in solid tumors. Moreover, aptamer synthesis is easier than antibody production, and aptamers could be easily conjugated with chemical or functional moieties. First GCPII aptamers, A9 and A10, were selected by

Lupold et al. on the basis of their ability to inhibit GCPII enzymatic activity<sup>107</sup>. A9 is functioning as a non-competitive inhibitor, while A10 is functioning as a competitive inhibitor. Both of these RNA sequences were used to produce shorter truncated aptamer versions with lower production costs. In 2013, Boyacioglu et al. selected DNA aptamer SZTI01 against GCPII ectodomain and developed dimeric aptamer complex optimal for doxorubicin targeted delivery<sup>108</sup>. Other DNA aptamers, A12, B1, and Apt1, were selected through the cell-based SELEX approach<sup>109,110</sup>.

For PET/SPECT imaging, A10 derived aptamer was radiolabeled with <sup>64</sup>Cu, however, *in vivo* PET imaging was not performed yet<sup>111</sup>. For other techniques, CT, MRI, and optical imaging, conjugates of aptamers with gold nanoparticles, SPIONs, or near-IR fluorophore were engineered<sup>112-114</sup>.

Since A10 and A9 aptamers possess inhibitory activity, they have a certain therapeutical potential. *In vivo* studies confirmed the anti-metastatic activity of A9g, A9 derived aptamer<sup>114</sup>. In the therapeutics area, aptamer conjugates are being developed for delivery of RNAi modulators, CRISPR/Cas9, toxins, chemotherapeutics, and nanoparticles<sup>115-119</sup>. Bispecific aptamers are engineered to enable recruitment of activated T-cells to the tumor site<sup>120</sup>.

### 1.2.3. Small-molecule inhibitors

Another branch of therapy/imaging approach is development of inhibitors that bind to the active site of the enzyme<sup>121</sup>. The first inhibitor with a high affinity and selectivity towards GCPII, 2-PMPA, was synthesized before the first high resolution structure of the GCPII was published<sup>122</sup>. Its design was based on the fact that the known natural substrate of GCPII NAAG possesses the C-terminal glutamate moiety and that zinc atoms at the active site are important for catalytical activity, so the inhibitor should have glutamate-derived moiety and a zinc-chelating group. Since the crystal structure of GCPII was solved, a novel era of structure-assisted inhibitor design has started. All existing inhibitors share common features and typically are made from the following parts – P1' moiety interacting with the S1' pocket (which is described in the chapter 1.3.1), a zinc-chelating group substituting the peptide bond, and an effector moiety interacting with the S1 pocket (also described in the chapter 1.3.1). Inhibitors are classified according to their zinc-binding group.



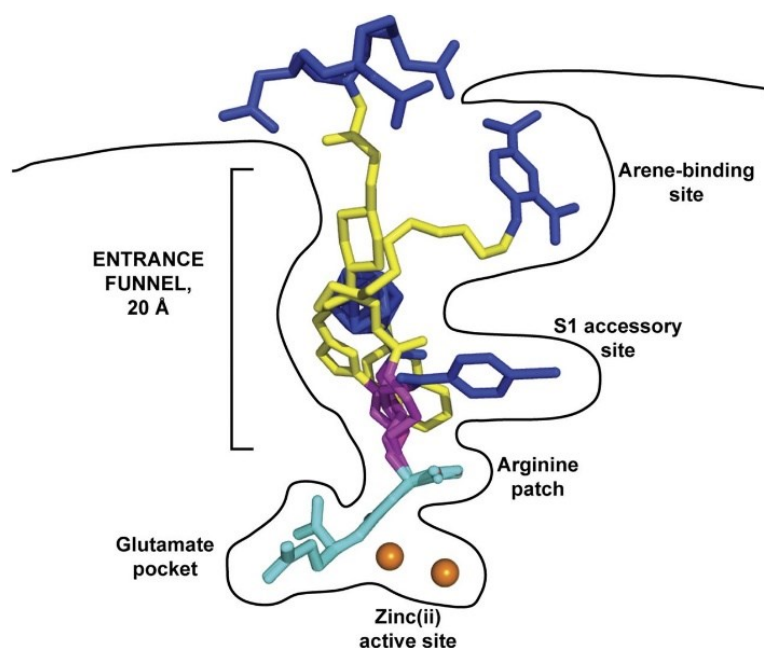


**Figure 2. Glu-ureido–based inhibitors within binding cavity of GCPII**

Complexes between GCPII and 4 Glu-ureido–based ligands are superimposed on corresponding  $C\alpha$  atoms of the protein. Although there is complete structural overlap of pharmacophore modules (cyan), positioning of flexible proximal linker (magenta), functional spacer (yellow), and effector moiety (blue) is divergent within (and outside) amphipathic entrance funnel. Zinc ions are shown as orange spheres. GCPII–inhibitor complexes used were DCIBzL (PDB code 3D7H), ARM-P4 (PDB code 2XEG), carborane (PDB code 4OME), and PSMA-617 (unpublished data). Reproduced from Kopka, K., Benešová, M., Bařinka, C., Haberkorn, U. & Babich, J. Glu-Ureido-Based Inhibitors of Prostate-Specific Membrane Antigen: Lessons Learned During the Development of a Novel Class of Low-Molecular-Weight Theranostic Radiotracers. *J. Nucl. Med. Off. Publ. Soc. Nucl. Med.* **58**, 17S-26S (2017)<sup>139</sup>.

### 1.2.3.1. Phosphorus-based inhibitors

Phosphorus-based inhibitors mimic the transition state of a GCPII substrate. The first inhibitor belonging to that group and the first selective GCPII inhibitor ever is 2-PMPA (2-(phosphonomethyl)pentanedioic acid) that has pentanedioic moiety at the P1' position and the phosphonate group as a zinc chelator<sup>122</sup>. It behaves as a competitive inhibitor and shows 300 pM value of  $IC_{50}$ <sup>123</sup>. Structure–activity relationship studies with 2-PMPA allowed the design of other potent inhibitors, including VA-033 and phosphinate-based GPI 5232<sup>124,125</sup>. 2-PMPA was used for investigations of the neuroprotective impact of GCPII inhibition in preclinical models<sup>63</sup>. However, 2-PMPA is a highly hydrophilic molecule, and, consequently, shows poor bioavailability and penetration of the blood-brain barrier. Efforts to prepare more lipophilic but

still potent compounds based on 2-PMPA did not lead to any significant improvement of the pharmacokinetic profile<sup>125,126</sup>. Nevertheless, Majer et al. synthesized 2-PMPA prodrugs with the masked zinc-binding group exhibiting satisfactory oral bioavailability<sup>127</sup>.

Pseudo-irreversible phosphoramidate-based inhibitors with both a hydrophobic moiety and a COOH group at the P1 position were presented by Berkman's group<sup>128</sup>. They were found to induce GCPII internalization *in vitro* and, thus, could be beneficial therapeutic agents. Phosphoramidates show higher binding affinity towards GCPII than matching phosphonates due to additional hydrogen bonds formed at the active site<sup>129</sup>.

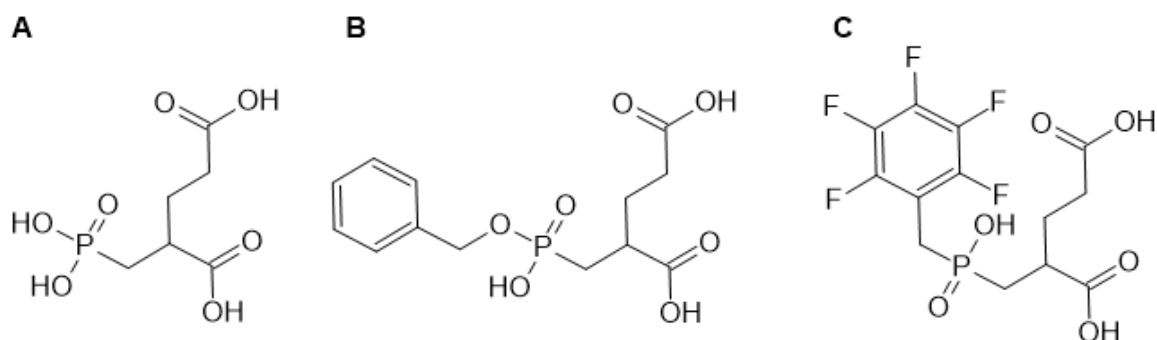


**Table 1. Chemical structure of selected phosphorus-based GCPII inhibitors**

A. 2-PMPA, 2-(phosphonomethyl)pentanedioic acid

B. VA-033, 2-[[hydroxy(phenylmethoxy)phosphoryl]methyl]pentanedioic acid

C. GPI5232, 2-[[hydroxy-[(2,3,4,5,6-pentafluorophenyl)methyl]phosphoryl]methyl]pentane-dioic acid

### 1.2.3.2. Thiol-based inhibitors

Thiol-based inhibitors were derived in an attempt to replace the highly polar zinc-binding phosphorus-based group with a more lipophilic one. 2-PMPA analog with the thiol zinc-binding group, 2-MPPA (2-(3-mercaptopropyl)pentanedioic acid), exhibits  $IC_{50} = 90$  nM and better oral bioavailability<sup>130</sup>. Its effectivity after peroral administration was shown in several preclinical models. 2-MPPA was found to be safe and relatively well tolerated at relevant plasma concentrations in phase I of clinical studies<sup>131</sup>. However, 2-MPPA is a relatively low potency inhibitor. Another issue is the immunoreactivity associated with thiol compounds. 2-MPPA was used as a template for development of inhibitors with benzyl- or indole-containing moieties at the P1' position<sup>132,133</sup>. Despite showing remarkable structural differences from the physiological substrate NAAG, such inhibitors are more potent than 2-

MPPA (lowest IC<sub>50</sub> values 2 and 22 nM)<sup>133,134</sup>. Indole-containing compounds are also the first achiral inhibitors of GCPII.

Glutamyl sulfonamide-based inhibitors contain a tetrahedral zinc-binding group that is structurally close to phosphoramidate, but, unlike phosphoramidate, is neutral at the neutral pH. However, existing inhibitors of that type are low (μM) potent<sup>135</sup>. Potency of sulfamide-based inhibitors is not optimal either<sup>136</sup>.

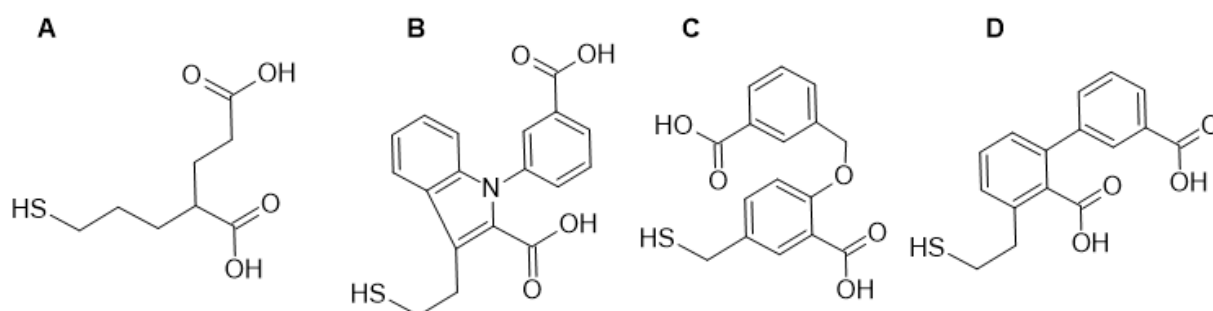


**Table 2. Chemical structure of selected thiol-based GCPII inhibitors**

- A. 2-MPPA, 2-(3-mercaptopropyl)pentanedioic acid  
 B. 1-(3-carboxyphenyl)-3-(2-sulfanylethyl)indole-2-carboxylic acid  
 C. 2-[(3-carboxyphenyl)methoxy]-5-(sulfanylmethyl)benzoic acid  
 D. 2-(3-carboxyphenyl)-6-(2-sulfanylethyl)benzoic acid

### 1.2.3.3. Urea-based inhibitors

Urea-based inhibitors contain a planar urea zinc-binding group mimicking the peptide bond of the substrate and connecting the P1' glutamate with the P1 moiety<sup>137</sup>. ZJ-43, (2S)-2-[[[(1S)-1-Carboxy-3-methylbutyl]carbamoylamino]pentanedioic acid, possesses nanomolar potency and has shown its utility in preclinical models of neurological disorders<sup>62,66,138,139</sup>. DCIBzL, (2S)-2-[[[(1S)-1-carboxy-5-[(4-iodobenzoyl)amino]pentyl]carbamoylamino]pentanedioic acid, possessing the haloaromatic moiety at the P1 position, is the most potent ever synthesized GCPII inhibitor with the K<sub>i</sub> value equal to 10 pM<sup>140</sup>. Urea-based inhibitors, as well as phosphorus-based compounds, are highly polar and thus poorly bioavailable, but are broadly exploited for prostate cancer imaging<sup>141</sup> or therapy, for example, in a form of PSMA-617 and PSMA-I&T<sup>142,143</sup>. Attempt to decrease hydrophilicity of urea-based compounds led to the development of inhibitors with carborane moieties<sup>144</sup>. Such compounds also possess a potential

for boron neutron capture therapy of prostate cancer<sup>145</sup>. ZJ-43 was used as a template for carbamate-containing inhibitors<sup>146</sup>.

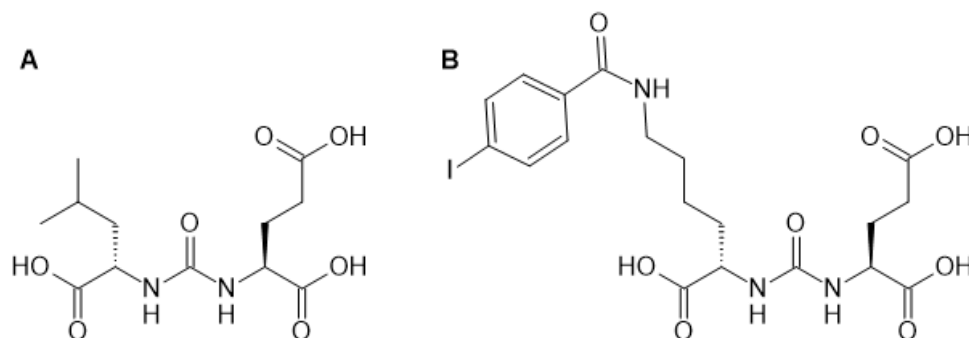


**Table 3. Chemical structure of selected urea-based GCPII inhibitors**

**A.** ZJ-43, (2S)-2-[[[(1S)-1-Carboxy-3-methylbutyl]carbamoylamino]pentanedioic acid

**B.** DCIBzL, (2S)-2-[[[(1S)-1-carboxy-5-[(4-iodobenzoyl)amino]pentyl]carbamoylamino]pentanedioic acid

#### 1.2.3.4. Hydroxamic acid-based inhibitors

2-(Hydroxycarbamoylmethyl)pentanedioic acid, a 2-PMPA analog with hydroxamic acid as the zinc-binding group, is relatively low potent ( $IC_{50} = 220\text{nM}$ )<sup>147</sup>. Nevertheless, compounds (enantiomers) with the C-terminal moiety substituted by an aromatic one exhibit higher affinity (the lowest  $IC_{50}$  value equal to 44nM) and are orally bioavailable<sup>148</sup>. The C-terminal moiety of those inhibitors is not positioned into the S1' pharmacophore pocket as expected but instead is resident in the S1 pocket (what explains why it is tolerated even though being noncanonical). For further improvement, prodrugs with the masked zinc-binding group have been developed. The most potent one, *para*-acetoxybenzyl-based, increases bioavailability of the original inhibitor 5-fold<sup>149</sup>.

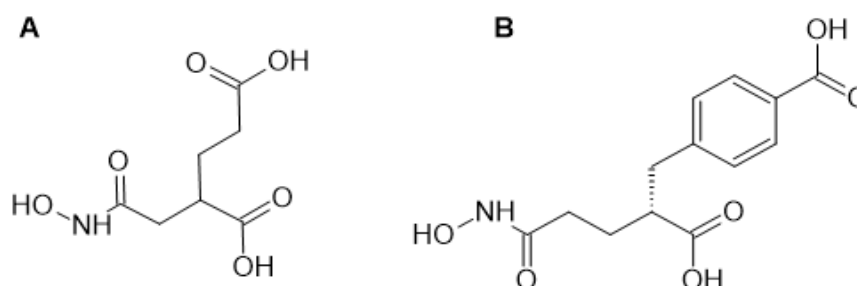


**Table 4. Chemical structure of selected hydroxamate-based GCPII inhibitors**

**A.** 2-(hydroxycarbamoylmethyl)pentanedioic acid

**B.** 4-[(2R)-2-carboxy-5-(hydroxyamino)-5-oxopentyl]benzoic acid

Knowledge of the structure and catalytic mechanism is relevant for the development of all above-mentioned targeting agents. Structural characteristics of GCPII and reaction mechanism of GCPII-catalyzed cleavage are described in the following chapters 1.3 and 1.4.

### 1.3. Structural characteristics of GCPII

GCPII is a type II transmembrane glycoprotein that consists of a short N-terminal cytoplasmic tail (amino acids 1-18), a single transmembrane helix (amino acids 19-43), and a large C-terminal extracellular part (amino acids 44-750). A tertiary (and quaternary) structure is known only for the extracellular part, which resembles the 3D fold of the transferrin receptor. It was firstly published in 2005 by Davis et al.<sup>150</sup>, however at a low, 3.5 Å, resolution. Then, in 2006, the structure of GCPII ectodomain complexes with several ligands was published at higher resolution by Mesters et al.<sup>151</sup>, and ligand-free high-resolution structure of the GCPII ectodomain was published in 2007 by Barinka et al.<sup>152</sup>.

Three structural domains of the extracellular GCPII portion could be distinguished – protease-like, apical, and C-terminal (helical) domains.

The protease-like domain contains amino acids 57-116 and 352-590. It is composed of a 7-stranded mixed  $\beta$ -sheet surrounded by 10  $\alpha$ -helices and closely resembles folds of bacterial aminopeptidases *Aeromonas proteolytica* (PDB code 1AMP<sup>153</sup>) and *Streptomyces griseus* (PDB code 1XJO<sup>154</sup>), both of which also belong to the same M28 metallopeptidase family<sup>151</sup>. Between the antiparallel 1<sup>st</sup> and 2<sup>nd</sup> strands of the  $\beta$ -sheet,  $\beta$ 1 and  $\beta$ 9, the apical domain is inserted. Another part of the otherwise relatively rigid protease-like domain is a flexible entrance lid – the Trp541-Gly548 segment, which could adopt either closed or open conformation<sup>155</sup>. Its conformational change is facilitated by the peptide bond flip between residues Asn540 and Trp541 and flexibility of Gly548. In the closed conformation, the entrance lid has a secondary structure of a single  $\alpha$ -helix and prohibits communication between the external space and the substrate-binding site. This conformation is observed in complexes of GCPII and small ligands. In complexes of GCPII with larger bulkier ligands, such as foyl-poly- $\gamma$ -glutamate, the entrance lid adopts open conformation, which is characterized by the absence of the rigid secondary structure. As such ligands could also be processed by GCPII<sup>156</sup>, the conformation of the entrance lid does not affect enzyme activity<sup>157</sup>.

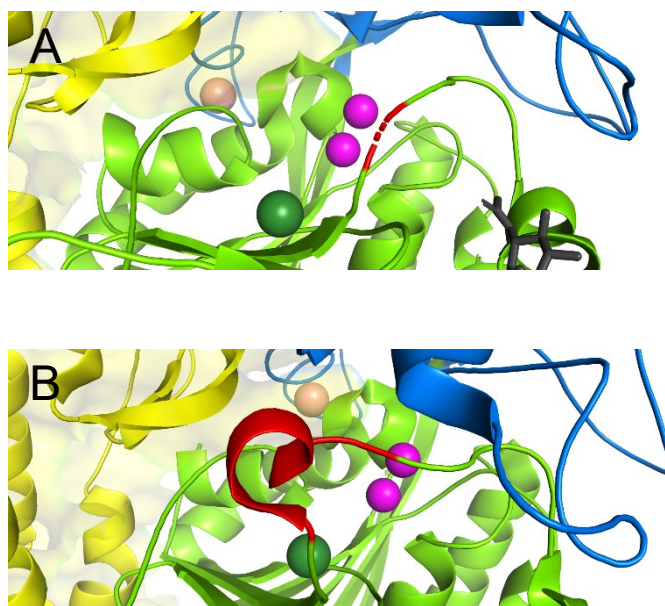


**Figure 3.**

- A. Unstructured entrance lid (red)**  
Surrounding environment is pictured in the same manner as at the Figure 7. PDB code 2OOT.
- B. Structured entrance lid**  
Surrounding environment is pictured in the same manner as at the Figure 7. PDB code 3BHX.

When the entrance lid is in the open conformation, the arene-binding site (formed by the indole group of Trp541 and guanidinium groups of Arg463 and Arg511) is accessible. The arene-binding site could enhance affinity towards arene-containing inhibitors *via* stacking interactions<sup>158</sup>.

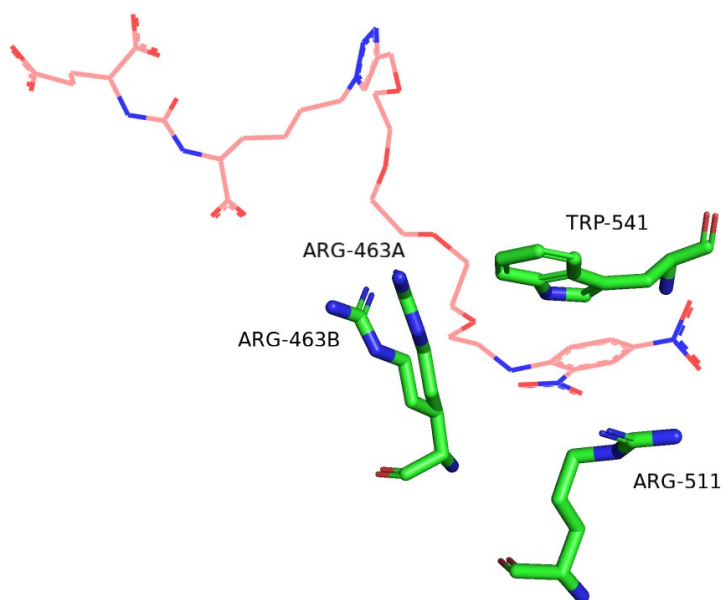


**Figure 4. Arene binding site**

Ligand ARM-P4 (represented with lines) engaged in stacking interactions with residues Arg511 and Trp541 of arene binding site (represented with sticks) Arg463 is presented by two rotamers. PDB code 2XEG.

The apical domain is formed by residues 117-351. It creates an entrance funnel between domains by covering the active site<sup>151</sup>. The apical domain is formed by central (3+4)-stranded  $\beta$ -sandwich surrounded with four  $\alpha$ -helices. The third strand of the  $\beta$ -sandwich is followed by a type II polyproline helix consisting of four proline solvent-exposed residues – Pro146-149<sup>151</sup>.

PxxP motif is known to play a role in protein-protein interactions *via* recognition by SH3 domain<sup>159, 160</sup>, however, it is not clear whether it is true for GCPII<sup>157</sup>.

The C-terminal, also known as helical, domain (amino acids 591-750) contains an Up-Down-Up-Down bundle, which is formed by helices  $\alpha 15$ ,  $\alpha 17$ ,  $\alpha 18$ - $\alpha 19$ , and  $\alpha 20$ , and a small two-turn helix  $\alpha 16$  that is located on the loop after helix  $\alpha 15$  and is perpendicular to the other helices<sup>151</sup>. The helix  $\alpha 18$  is followed by two loops containing residues 676-690 and 692-704. The first loop is interacting with the protease-like and apical domains through the H-bonds, and Val690 returns to form the C-cap of the helix  $\alpha 18$ <sup>151</sup>. The residues from second loop, called glutarate sensor, Lys699 and Tyr700, are involved in ligand binding at the active site.

### 1.3.1. Binding cavity

Large (about 1100 Å<sup>2</sup>) binding cavity<sup>150</sup> is formed by interfaces of all three domains. It is divided by the active site into two – S1, also known as the non-pharmacophore, and S1', the pharmacophore, – pockets<sup>161</sup>. Preferences of the GCPII towards physicochemical characteristics of its substrates and inhibitors are given by the amino acid residues shaping S1 and S'<sup>161</sup>.

The non-pharmacophore pocket of the GCPII is represented by a shape-shifting entrance funnel of a depth of 20 Å with a narrow base (diameter 8 Å) and 20 Å wide entrance rim<sup>151,157</sup>. The pocket is defined by residues Ser454, Glu457, Asp465, Asn519, Gly548, Tyr549, Tyr552, and a stack of three arginines – Arg463, Arg534, and Arg536, – known as the arginine patch, from which Arg463 is located on the  $\beta$ -strand  $\beta 13$  of the protease-like domain, while Arg534 and Arg546 are located on antiparallel  $\beta 14$ <sup>151</sup>.

The arginine patch is situated at the distance of 6.5–12.7 Å from the nearest Zn<sup>2+</sup> ion and determines the preference for the negatively charged moieties, as are glutamate and aspartate, at the P1 position of a substrate<sup>152,162</sup>. An important feature of the arginine patch is a relative flexibility of Arg463 and Arg536. Arg534 is maintained in energetically costly position by the interaction with the Cl<sup>-</sup> ion (that is also coordinated by Arg580, Asp453, Asn451, and two water molecules)<sup>151</sup>. The dependence of GCPII hydrolytic activity on the presence of chloride anions was shown by Robinson et al. in 1987<sup>17</sup>. Chloride ion prevents Arg534 from changing the conformation to one more favorable, which presumably is not able to form direct contact with the substrate upon its binding, unlike the conformation characteristic for Arg534 interacting

with  $\text{Cl}^{-155,151}$ . Arg463 forms a hydrogen bond with the  $\gamma$ -carboxylate of Glu457<sup>152</sup>. Arg536 could adopt two positions – binding or stacking. In the stacking position, Arg536 is not available for the substrate binding, and its guanidium group is located between guanidium groups of Arg463 and Arg536<sup>155</sup>.

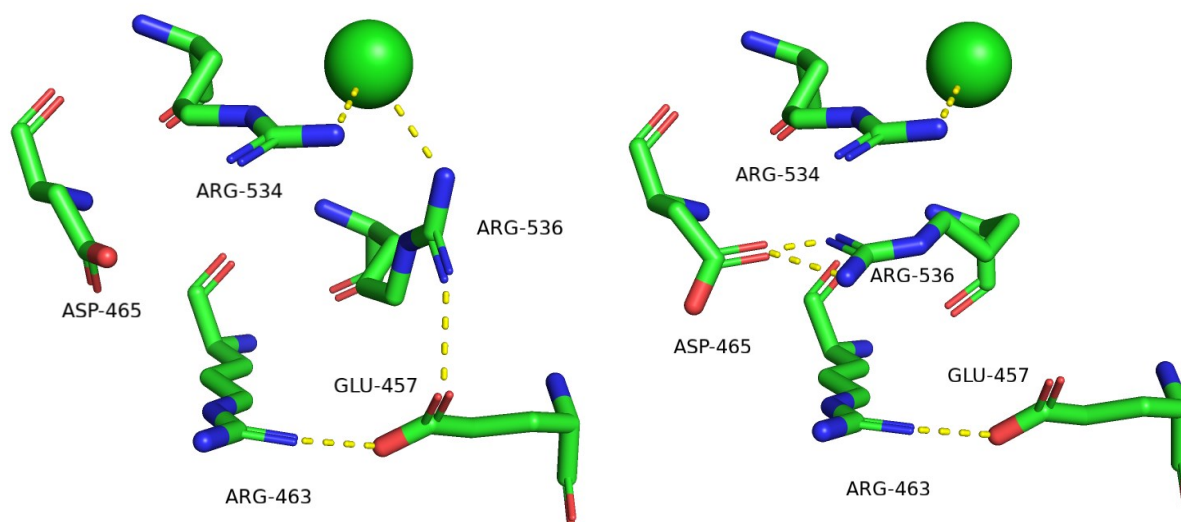


**Figure 5. Arginine patch**

Left – binding position of Arg536. Arg536 is engaged in interactions with chloride anion (dark green sphere) and Glu457. PDB code 2OOT.

Right – stacking position of Arg536. Arg536 is stacked between residues Arg463 and Arg534 and stabilized by interaction with Asp465. PDB code 2OOT.

Stacking of the guanidium groups is further stabilized by ionic interactions with the carboxylate of Asp465<sup>152</sup>. Change of the Arg536 position to the binding conformation is accompanied by a 4.5 Å shift of the guanidium group<sup>155</sup>. Here, Arg536 is stabilized primarily by interactions with Glu457 and the same  $\text{Cl}^{-}$  ion that stabilizes Arg534. Rearrangement of Arg536 and Arg463 leads to the appearance of the cavity with parameters 8.5 Å x 7 Å x 9 Å, known as the S1 accessory hydrophobic pocket<sup>163</sup>.



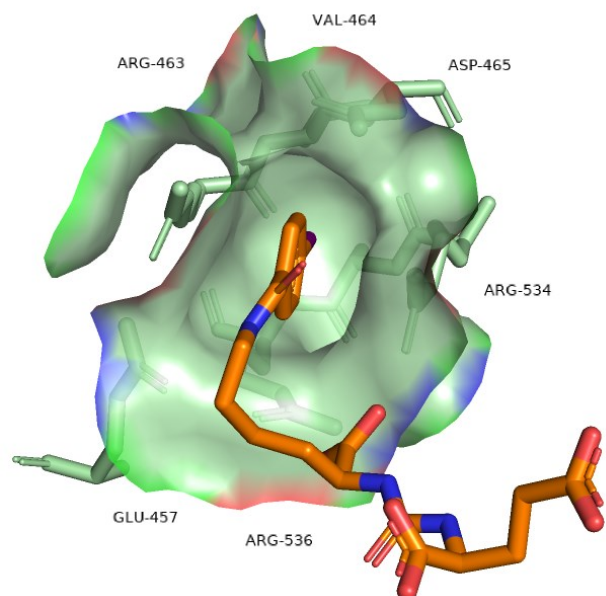


**Figure 6. Accessory hydrophobic pocket**

DCIBZL effector moiety (orange sticks) placed into the accessory binding site. Protein residues Glu457, Arg463, Val464, Asp465, Arg534, and Arg536 are represented with salad green sticks and semitransparent surface. PDB code 3D7H.

The pharmacophore pocket, which for the most part defines specificity and affinity of GCPII towards substrates, has dimensions 8 x 8 x 8 Å and is shaped by residues Phe209, Arg210, Asn257, Glu424, Glu425, Gly427, Leu428, Gly518, Lys699, and Tyr700<sup>164,151,152</sup>. It could slightly change shape at the basis of induced-fit mechanism, for example, by changing the spatial localization of residues Phe209, Asn257, Gly518, but is more rigid and restricted compared to non-pharmacophore pocket<sup>164</sup>. Limitation of the S1' pocket plasticity arises from the overall fold of the extracellular part of GCPII, as all three domains contribute to its shape. The distance between residues Phe209 and Leu428 remains constant (8 Å), defines the pocket width and restricts the substrate/inhibitor size<sup>164</sup>. The most flexible part of the pocket is the glutarate sensor that could drastically change its structure upon substrate binding.

The pharmacophore pocket has an amphipathic character, and its preference to substrates with C-terminal glutamate is given by arising polar and Van der Waals interactions combined with hydrophobic effect<sup>164</sup>. As it was discussed earlier in the chapters 1.1 and 1.2, the only known GCPII physiological substrates harbor glutamate at their C-terminus, and, consistently, most of the existing inhibitors are glutamate-derived molecules.

The active site of GCPII is organized around two zinc ions. One of them, catalytic, is coordinated by residues His553 and Glu425, other, co-catalytic, is coordinated by His377 and Asp453<sup>151</sup>. Ions are bridged in a bidentate manner by Asp387. The peptide bond between Asp387 and the next residue, Pro388, is in cis conformation. Both ions are also bridged by the

hydroxide anion, which forms a hydrogen bond with the conserved residue Glu424 that is acting as a proton shuttle during cleavage of a substrate<sup>152</sup>.

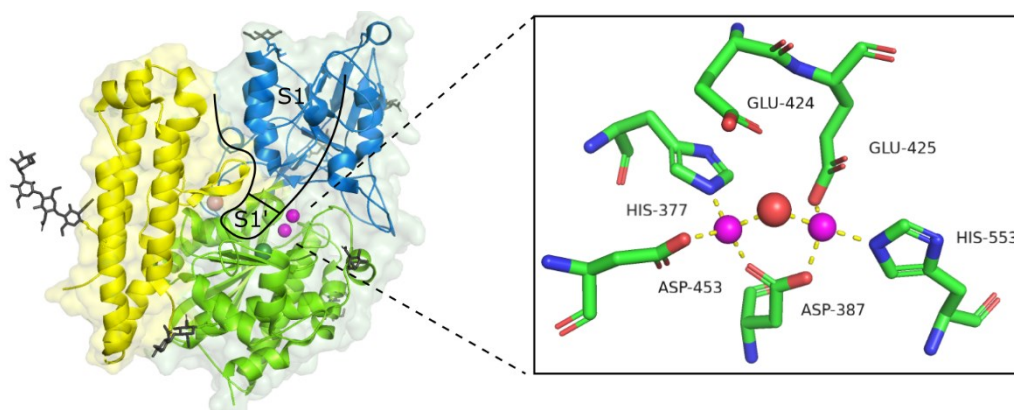


**Figure 7.**

- A.** GCPII ectodomain, individual (sub)domains are presented as cartoon colored with light green (protease-like domain), blue (apical domain), and yellow (C-terminal domain). Carbohydrate moieties linked to Asn76, Asn121, Asn140, Asn195, Asn476, and Asn638 are pictured in grey color. Zinc, chloride, and calcium ions are presented as spheres and colored magenta, dark green, and coral, respectively. The binding cavity is schematically represented with the black line, pharmacophore and non-pharmacophore pockets are signed as S1' and S1. PDB code 2O0T.
- B.** Coordination of active site zinc ions (magenta spheres) with amino acids Glu425, His377, Asp387, Asp453, and His553 (represented with sticks) and hydroxide anion (red sphere). PDB code 2O0T.

### 1.3.2. Posttranslational modifications

Glycosylation is a common posttranslational modification for type II transmembrane proteins and takes place in the endoplasmic reticulum and the Golgi apparatus. It could affect protein folding, sorting, stability, and enzymatic activity to various extent. Glycosyl moieties, mostly N-linked to the protein<sup>165</sup>, are estimated to make about 20% of the GCPII molecular weight<sup>166</sup>. In total, ten N-glycosylation sites (Asn-X-Ser/Thr sequence where X is any amino acid except proline) exist in GCPII – at the residues Asn51, Asn76, Asn121, Asn140, Asn153, Asn195, Asn336, Asn459, Asn476, and Asn638<sup>1,167</sup>. Total deglycosylation with the Peptide:N-glycosidase F or protein expression in the medium containing tunicamycin, a known inhibitor of the first N-glycosylation step, lead to complete inhibition of the enzymatic activity of GCPII<sup>162,165</sup>. The latter also affects GCPII folding, although none of the individual glycosylation sites is crucial for that by itself<sup>167</sup>. Site-directed mutagenesis shows that

individual N-glycosylation sites have a different influence on GCPII enzymatic activity: asparagines 121, 140, 153, 195 and, especially, 638 are the most crucial glycosylation sites<sup>167</sup>. Oligosaccharide chain on the Asn638 is actually the most rigid, since, typically, four saccharide units could be modeled into electron density maps in crystal structures (for other sites, the number is usually two), and plays role in forming of GCPII dimers (further discussed in the chapter 1.3.3)<sup>157</sup>.

Another property differently affected by individual glycosylated sites is protein stability, for which N-glycosylation of Asn336, Asn459, and Asn476 is important<sup>165</sup>.

### 1.3.3. Quaternary structure

At the quaternary level, the native conformation of GCPII is a noncovalent homodimer. Homodimerization was found to be obligatory for the enzymatic activity of GCPII, although active sites on both monomers are mutually independent<sup>168</sup>.

Dimerization is driven by the extracellular part of GCPII<sup>168</sup>. Dimerization interface of 2457Å<sup>2</sup> is formed mainly by residues from the C-terminal domain of one monomer and residues from protease-like and apical domains from another<sup>151</sup>. Two salt bridges are formed between the  $\alpha$ 18 helices of C-terminal domains by Arg662 of the one monomer and Asp666 of the other<sup>151</sup>. In addition, each GCPII monomer contains a Ca<sup>2+</sup> cation that is coordinated by a water molecule and residues Glu433, Glu436, Thr269, and Tyr272 from both protease-like and apical domains, thus holding them together and stabilizing the Leu268–Arg280 loop, which interacts with a surface of  $\alpha$ 20 helix from the second GCPII protomer<sup>169</sup>. The sidechain of Glu276 forms hydrogen bonds with two units of the carbohydrate chain linked to the abovementioned Asn638 from the second monomer, contributing to the formation of a dimer.

### 1.4. Mechanism of catalysis

In 2009, Klusák et al. described the reaction mechanism of GCPII-catalyzed cleavage of the peptide bond in NAAG, one of the known physiological substrates of GCPII (for more information, see chapter 1.1.1), based on QM/MM calculations and crystallographic structures of complexes GCPII/glutamate<sup>151</sup>, GCPII/transition state mimetics<sup>164,155</sup> and a complex of GCPII inactive mutant with NAAG<sup>170</sup>. The reaction coordinate of that process reveals two transition states, formation of the second being the rate-determining step of the reaction, and one intermediate complex.

During the catalysis, Glu424 plays a role of a proton shuttle, transferring the first proton from the activated water molecule to the peptide bond nitrogen and accepting the second proton from the remaining OH<sup>-</sup> anion. The same type of behavior was proposed for corresponding Glu residues in active sites of aminopeptidases from *Aeromonas proteolytica* and *Streptomyces Griseus*, which catalytic domains are highly homologous to the one of GCPII<sup>171,172</sup>.

The peptide bond in the substrate is planar. NH group of this bond forms hydrogen bond with the carbonyl oxygen of Gly518, the same amino acid that stabilizes Glu424. The carboxyl group is polarized by interaction with the catalytic Zn<sup>2+</sup> ion and interaction with Tyr552, which is stabilized by the side chain of Arg210. The carboxyl group is shifted from planarity and elongation of the distance between zinc ions occurs. Sp<sup>3</sup> hybridization of the nitrogen from the amino group is stabilized by interaction with a proton from the carboxyl group of Glu424, which now changes its position. The scissile peptide bond carbon is activated and forms a bond with the oxygen from OH<sup>-</sup> bridging zincs. A proton from Glu424 is transferred to the peptide bond nitrogen, a proton from OH<sup>-</sup> ion is transferred to Glu424, and cleavage of the peptide bond occurs. The reaction cycle is finished with an influx of a water molecule into bridging position, where it is activated by proton abstraction. The proton is accepted by Glu424<sup>170</sup>.

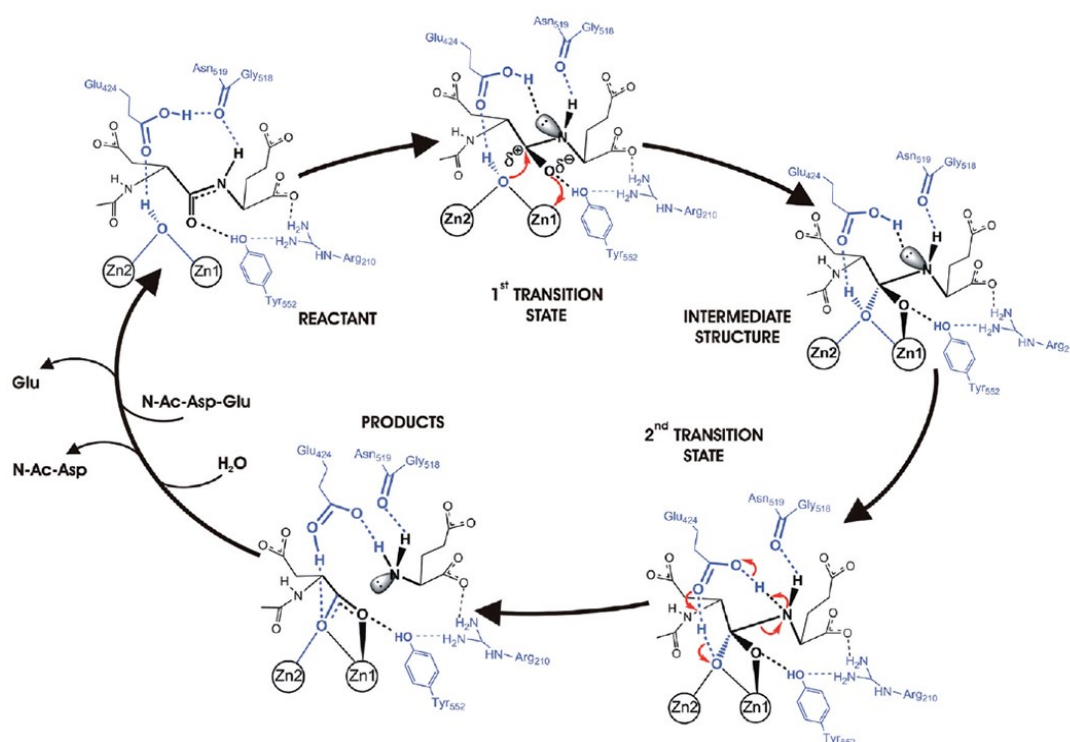


### **Figure 8. GCPII reaction cycle depicting important steps/structures throughout the reaction pathway**

The proposed reaction mechanism was obtained by QM/MM calculations and is consistent with the crystal structures of NAAG bound in the active site of the E424A mutant of GCPII, as well as with structures of the transition state analogue, and enzyme-product complexes reported previously. Reproduced from Klusák, V., Barinka, C., Plechanovová, A., Mlcochová, P., Konvalinka, J., Rulísek, L., & Lubkowski, J. Reaction mechanism of glutamate carboxypeptidase II revealed by mutagenesis, X-ray crystallography, and computational methods. *Biochemistry*, **48**(19), 4126–4138 (2009)<sup>170</sup>.

The activation barrier of reaction is predicted to be about 22 kcal/mol (estimated error 5 kcal/mol)<sup>170</sup>. Experimentally determined values of turnover number and Michaelis constant are  $k_{\text{cat}} = 1.1 \text{ s}^{-1}$ , and  $K_{\text{m}} = 1.2 \text{ }\mu\text{M}$  at pH 7.4<sup>173</sup>. The pH optimum for the reaction lies between 6.0 – 8.0<sup>162</sup>.

#### **1.5. Existing GCPII activity assays**

Interest in the development of GCPII inhibitors for imaging/therapy purposes dictates the need in the *in vitro* assay for their screening and evaluation. Up to date, various methods for studies of GCPII activity and its inhibition by different ligands *in vitro* have been developed. However, no direct continuous assay was introduced for inhibitor evaluation yet. Most of the methods are also not well suited for high-throughput screening of chemical libraries in search of potent inhibitors.

##### **1.5.1. Radioenzymatic assay**

The radioenzymatic assay is the oldest *in vitro* GCPII assay considered a prime method for GCPII activity and inhibition studies<sup>17</sup>. It is based on monitoring hydrolysis of NAAG radiolabeled with tritium. Uncleaved NAAG and [<sup>3</sup>H]glutamate are separated using an ion-exchange column, and the latter is eluted with 1M formate. Radioactivity that corresponds to released [<sup>3</sup>H]glutamate is consequently determined on scintillation counter<sup>174</sup>. The assay is highly sensitive and has low false-positivity rates, however, at the same time costly, time-consuming, and producing hazardous waste, amount of which nevertheless could be reduced by the usage of solid scintillation counting method instead of liquid<sup>175</sup>.

##### **1.5.2. Fluorescence end-point assay**

Another possibility to study GCPII activity is fluorescent detection of cleavage products. To enable that, derivatization agent as *o*-phthalaldehyde (OPA) could be added to the reaction mixture upon incubation<sup>162,173</sup>. In the alkaline environment, OPA reacts with NH<sub>2</sub>

group of the cleaved C-terminal amino acid (glutamate) producing a strong fluorescent signal at 455 nm, which is proportional to amino acid concentration<sup>176,177</sup>.

For measurements of kinetic parameters, preincubated with OPA glutamate is detected by HPLC (for more information see chapter 1.5.3).

### 1.5.3. HPLC-based assay

The HPLC-based assay utilizes hydrolysis of a synthetic GCPII substrate, which is based on natural substrates and bears a chromophore moiety suitable for HPLC detection. N-(4-phenylazobenzoyl)-glutamyl- $\gamma$ -glutamic acid, PABG $\gamma$ G, was found to be optimal for that purposes<sup>178</sup>. The reaction of GCPII with PABG $\gamma$ G is stopped after 15 minutes, the substrate and the cleavage product are then separated on a reverse-phase HPLC column and detected by absorbance at 325 nm<sup>179</sup>. This assay is sensitive (down to 10 nM limit for the substrate or its product), does not produce hazardous waste, has low-false positive rates, but is time-consuming.

An older HPLC-based assay exploited pre-column product derivatization with OPA or AccQ-Fluor instead of having a chromophore-bearing substrate<sup>162,180</sup>. However, such method shows low sensitivity and fails to measure  $K_m$  values under 5  $\mu$ M detection limit (1  $\mu$ M in case of AccQ-Fluor)<sup>155,162</sup>.

Recently, UPLC-based assays, one employing NAAG as a substrate and using product derivatization, and the other, employing oxidized folyl-poly- $\gamma$ -glutamates as substrates, were developed<sup>38</sup>. Both of them are sensitive and possess detection limits 20-30 nM and 10 nM, respectively.

### 1.5.4. Fluorescence polarization assay

Fluorescence polarization assay is based on the usage of a fluorescent ligand, TMR-X-Lys-urea-Glu, which binds to the GCPII active site<sup>181</sup>. Formation of the GCPII/TMP-X-Lys-urea-Glu complex changes fluorescence polarization (from 50 to 380 mP) and decreases quantum yield from the probe, which could also be monitored as a complementary parameter to polarization. Competitive inhibitors could either displace TMR-X-Lys-urea-Glu from the active site or block its binding, leading to the decrease of polarization value. The assay is also suitable for screening of noncompetitive inhibitors, as they are also able to block binding of the probe. The assay is robust, relatively cheap, compatible with common solvents, conductible even at high salt concentrations, and well-suited for high-throughput screening. As the assay

lower limit is 20 nM, it is not suitable for characterization of more potent compounds with  $IC_{50}$  below this value.

#### **1.5.5. Amplex Red glutamic acid assay**

Amplex Red glutamic acid assay uses a commercially available kit (Thermo Fisher Scientific) that contains the reaction mixture including alanine, several enzymes (glutamate oxidase, glutamate-pyruvate transaminase, horseradish peroxidase), and the Amplex Red reagent, 10-acetyl-3,7-dihydroxyphenoxazine. NAAG is used as a substrate<sup>140</sup>. Cleaved glutamate is then oxidized to  $\alpha$ -ketoglutarate, producing  $NH_3$  and  $H_2O_2$ ,  $\alpha$ -ketoglutarate is transaminated, restoring glutamate, leading to multiple cycles of glutamate oxidation reaction and amplification of  $H_2O_2$  production<sup>182</sup>. HRP catalyzes the reaction of  $H_2O_2$  with Amplex Red reagent, giving rise to a fluorescence signal with intensity proportional to the concentration of cleaved glutamate<sup>183,184</sup>. The assay is sensitive (detection limit 10 nM), suitable to high throughput screening, but is expensive and has a high false-positive rate due to the presence of additional enzymes in the reaction mixture, oxidation of tested components by  $H_2O_2$ , and a following decrease of fluorescence signal<sup>181</sup>.

Similar enzyme-coupled assay commercial kits are PicoProbe™ glutamate carboxypeptidase II activity assay kit (BioVision) and glutamate carboxypeptidase II inhibitor screening kit (PromoCell).

#### **1.5.6. Fluorescence continuous assay**

An article presenting the only existing continuous method for GCPII enzymatic activity detection was published in 2019<sup>185</sup>. The method exploits an activable 5GluAF2MeTG probe, consisting of a glutamate moiety conjugated to the fluorophore 2-methyl TokyoGreen through the azoformyl linker. Fluorescence of the 2MeTG moiety is quenched by photoinduced electron transfer. After the cleavage of the linker by GCPII, the free fluorophore is highly fluorescent. 5GluAF2MeTG allows detection of GCPII enzymatic activity in living cells and could be useful for intraoperative detection of prostate carcinoma. However, the assay with this probe is not adapted for inhibitor measurement yet.

## 2. Aims

The main aim of this thesis was to develop the continuous GCPII activity assay. Specific aims were:

- To characterize biophysical parameters of designed fluorescent probes (GCPII substrates).
- To optimize kinetic measurements with the fluorescent probes using a microplate reader.
- To corroborate results of kinetic measurements obtained with a microplate reader using an HPLC-based detection.
- To crystallize complexes of fluorescent probes with an inactive GCPII mutant, solve, refine, and analyze corresponding structures.



### 3. Experimental part

#### 3.1. Materials

##### Chemicals

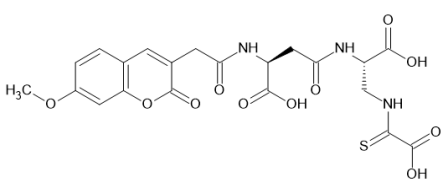
##### Provider companies

Acetonitrile	Honeywell
C <sub>12</sub> E <sub>8</sub> (dodecyloctaglycol)	Sigma-Aldrich Co.
Formic acid	Sigma-Aldrich Co.
7-Methoxycoumarin-4-acetic acid	Sigma-Aldrich Co.
NaCl	Lach-Ner, s. r. o.
PEG3350	Sigma-Aldrich Co.
Pentaerythritol propoxylate PO/OH 5/4	Sigma-Aldrich Co.
Trifluoroacetic acid	Sigma-Aldrich Co.
Tris-HCl	MP Biomedicals

rhGCPII and rhGCPIIE424M (extracellular part of recombinant human GCPII/GCPIIE424M) were available in our laboratory. They were prepared according to standard protocols<sup>162</sup>.

Compounds **1S-5S**, **1P** and **2P** (described in tab. 5) were obtained from the research group of prof. M. Schutkowski from Martin Luther University Halle-Wittenberg, Halle, Germany (synthesized by Dr. Marat Meleshin).

**Table 5. Substrates and corresponding standards**

Compound	Structure	Mw	Linker	Fluorophore	$\lambda_{EX}/\lambda_{EM}$ , nm
<b>1S</b>		523.5	No	7-Methoxy-coumarin-4-acetic acid	323/390

<b>2S</b>		636.6	Yes	7-Methoxy-coumarin-4-acetic acid	323/390
<b>3S</b>		537	No	7-Methoxy-coumarin-4-acetic acid	323/390
<b>4S</b>		650	Yes	7-Methoxy-coumarin-4-acetic acid	323/390
<b>5S</b>		684.5	Yes	BODIPY FI C1	503/509
<b>1P</b>		349.3	No	7-Methoxy-coumarin-4-acetic acid	323/390
<b>2P</b>		462.5	Yes	7-Methoxy-coumarin-4-acetic acid	323/390

Compounds **1S-5S** are examined fluorophore probes (GCPII substrates), compounds **1P** and

*2P* are the products of cleavage of compounds *1S* and *2S* respectively

## Instruments

Fluorescence spectrophotometer CLARIOstar (BMG Labtech GmbH, Ortenberg, Germany)

ThermoMixer (Eppendorf, Hamburg, Germany)

HPLC Prominence system (Shimadzu Corporation, Kyoto, Japan), Kinetex 2.6  $\mu\text{m}$  Polar C18 100 Å LC Column 50x3 mm (Phenomenex, Torrance, Canada)

D8 Venture diffractometer (Bruker Corporation, Germany)

MX14.2 beamline (BESSY II, Helmholtz-Zentrum Berlin, Berlin, Germany)

## 3.2. Methods

### 3.2.1. Fluorescence signal linearity – microplate readout

2-fold dilution series of each of the substrates *1S-5S* and corresponding standard compounds were prepared in the assay buffer comprising 50 mM Tris-HCl, 150 mM NaCl, 0.001% C<sub>12</sub>E<sub>8</sub> (dodecyltaglycol), pH 7.4 (later mentioned as the assay buffer), in a total volume of 50  $\mu\text{l}$ . 384-well low volume flat-bottom black polystyrene microplates (Corning) were used. To prepare the product of cleavage of *5S*, substrate *5S* was incubated with the excess of rhGCPII (100 $\mu\text{M}$  *5S*, 5 $\mu\text{M}$  rhGCPII) for 30 min at the ThermoMixer. Total cleavage was proved by HPLC (data not shown). Fluorescence intensity was measured using a CLARIOstar microplate reader for an hour. The experiment with each substrate was performed in triplicate twice. Data from the linear part of the curve were fitted using a linear regression equation in GraphPad Prism and are shown as mean  $\pm$  S.D. Quenching efficiency was calculated from the equations of linear regression ( $y=ax$ ) using the formula

$$\left(1 - \frac{a_{\text{quenched}}}{a_{\text{nonquenched}}}\right) \cdot 100\%, \quad (1)$$

where  $a_{\text{quenched}}$  and  $a_{\text{nonquenched}}$  are slope values for quenched and nonquenched compounds respectively. Details of experiments with individual substrates are summarized in tab. 6.

**Table 6. Design of fluorescence signal linearity assay experiments**

Substrate	Standard	Concentration range	$\lambda_{EX}/\lambda_{EM}$ , nm
1S	1P	49 nM - 25 $\mu$ M	323/390
2S	2P	49 nM - 25 $\mu$ M	323/390
3S	7-Methoxycoumarin-4-acetic acid	49 nM - 25 $\mu$ M	323/390
4S	7-Methoxycoumarin-4-acetic acid	49 nM - 25 $\mu$ M	323/390
5S	Completely cleaved 5S	49 nM - 25 $\mu$ M	493/ 545

### 3.2.2. Kinetic measurements – microplate readout

For each substrate, 2-fold dilution series were prepared in the assay buffer in 384-well low volume flat-bottom black polystyrene microplates (Corning), and rhGCPII was added to each well (total volume 20  $\mu$ l). Immediately after that microplate was inserted into a CLARIOstar microplate reader and the fluorescence intensity was measured for an hour. The experiment was performed twice in duplicates for each substrate. 2-fold dilution series of substrates were used as a control. 2-fold dilution series of compounds listed in the second column of tab 7. (same concentration range as a corresponding substrate) were used to produce a calibration curve by linear regression fit. For each concentration, velocity was calculated from the linear part of the measured curve by the formula

$$v = \frac{F_2 - F_1}{a \cdot c(E) \cdot \Delta t}, \quad (2)$$

where  $a$  represents the slope of the calibration curve,  $c(E)$  is the concentration of rhGCPII in  $\mu$ M,  $\Delta t$  is a time between first and last points of the chosen linear part of curve, and  $F_1$  and  $F_2$  is fluorescence intensity at the first and last points of the linear part of curve respectively.

For each concentration, conversion of the substrate was estimated using the formula

$$\eta = \frac{F_2 - F_0}{a \cdot c(S)}, \quad (3)$$

where  $a$  represents the slope of the calibration curve,  $c(S)$  is the initial concentration of the substrate in  $\mu\text{M}$ ,  $F_0$  is fluorescence intensity at the start of measurement, and  $F_2$  is fluorescence intensity at the last point of the linear part of the curve.

Calculated velocities were fitted using the Michaelis-Menten equation in GraphPad Prism. Data are shown as mean  $\pm$  S.D.

**Table 7. Design of kinetic assay experiments (microplate readout)**

Substrate	Standard	Substrate concentration range	rhGCPII concentration	$\lambda_{\text{EX}}/\lambda_{\text{EM}}$ , nm
1S	1P	49 nM-25 $\mu\text{M}$	500nM	323/390
2S	2P	49 nM-25 $\mu\text{M}$	500nM	323/390
3S	7-Methoxycoumarin-4-acetic acid	49 nM-25 $\mu\text{M}$	3 nM	323/390
4S	7-Methoxycoumarin-4-acetic acid	49 nM-25 $\mu\text{M}$	3 nM	323/390
5S	Completely cleaved 5S (prepared as described in section 3.2.1)	12 nM-6 $\mu\text{M}$	1 (1 <sup>st</sup> experiment) or 3 nM (2 <sup>nd</sup> experiment)	493/ 545

### 3.2.3. Kinetic measurements – HPLC readout

#### 3.2.3.1. Method development

5  $\mu\text{l}$  of 25  $\mu\text{M}$  substrate 5S with or without 5 $\mu\text{M}$  GCPII added was injected onto Kinetex 2.6  $\mu\text{m}$  Polar C18 100  $\text{\AA}$  LC Column (50x3 mm) using 4 different gradients (tab. 8) comprising solvents A (0.1 % formic acid in MilliQ water) and B (0.1 % formic acid in acetonitrile) with 0.6ml/min flow. Wavelengths for absorbance and fluorescence detection were selected as shown in tab. 9.

**Table 8. Examined HPLC gradients**

Time, min	Solvent B concentration, %			
	Gradient 1	Gradient 2	Gradient 3	Gradient 4
0.01	5	15	25	20
6.00	30	45	55	45
6.05	100	100	100	100
6.65	100	100	100	100
6.70	5	15	25	20
11.00	5	15	25	20

**Table 9. Absorbance and fluorescence wavelength settings**

Substrate	Absorbance, nm	Fluorescence $\lambda$ , nm
5S	503	Ex 503 Em 509

**3.2.3.2. Kinetic measurements**

2-fold dilution series of **5S** were prepared in the assay buffer in 96-well microplates (Thermo scientific), and to each well rhGCPII was added (total volume 100  $\mu$ l). After 30 min incubation, the enzymatic reaction was terminated with 0.1% TFA. Samples were injected into HPLC system (Shimadzu) using gradient 4. 2-fold dilution series of uncleaved **5S** with the same concentration range were used as a control. Conversion for each concentration was calculated on absorbance using the formula 4

$$\eta = \frac{A_{\text{product}}}{A_{\text{product}} + A_{\text{substrate}}} \cdot 100\%, \quad (4)$$

Where  $A_{\text{product}}$  and  $A_{\text{substrate}}$  are areas under a peak of the cleavage product and unprocessed substrate respectively. Velocities for each concentration was calculated using formula 5

$$v = \frac{\eta \cdot c(S)}{100 \cdot c(E) \cdot t}, \quad (5)$$

where  $t$  is a time of incubation. Calculated velocities were fitted using the Michaelis-Menten equation in GraphPad Prism. Data are shown as mean  $\pm$  S.D. Experimental settings are summarized in tab. 10.

**Table 10. Design of kinetic assay experiments (HPLC readout)**

Substrate	Gradient	Total reaction volume, $\mu\text{l}$	Substrate concentration range	RhGCPII concentration	Absorbance, nm
5S	4	100	12 nM-6 $\mu\text{M}$	3 nM	503

### 3.2.4. GCPII activity assay (measurement of $\text{IC}_{50}$ of T33D and DCIBzL)

For the carboxypeptidase activity assay, substrate **5S** was used. Triple dilution series of inhibitors (final concentration range 3 nM-500  $\mu\text{M}$  for T33D and 6 pM-100 nM for DCIBzL) were prepared in the assay buffer in 384-well flat-bottom black polystyrene microplates (Corning). After addition of rhGCPII to each well (final concentration 1 nM), samples were preincubated at ThermoMixer for 5 minutes. After that, **5S** was added to each well (final concentration 0.5  $\mu\text{M}$ ), and microplate was placed into a CLARIOstar microplate reader where the fluorescence intensity was measured continuously for an hour. Final volume of each reaction was 50  $\mu\text{l}$ . Mixture of 1nM rhGCPII and 0.5 $\mu\text{M}$  **5S** without any inhibitor was used as a control sample. Dilution series (concentration range 8nM – 0.5  $\mu\text{M}$ ) of cleaved **5S** were used as a calibration standard (prepared as described in section 3.2.1). For each concentration, velocity was calculated from the linear part of the measured curve by the formula 2. The experiment was performed five times for T33D and three times for DCIBzL in duplicates. Data were fitted using GraphPad Prism and are shown as mean  $\pm$  S.D.

### 3.2.5. Crystallization and data collection

Stock solution of rhGCPIIE424M (10mg/ml) was mixed with 50mM substrate in 20mM Tris-HCl, 150 mM NaCl, pH 8.0, at a 10:1 ratio. Enzyme/substrate complex mixture was mixed with the reservoir solution droplet. Crystals were grown by handing-drop method at 293 K and then vitrified in liquid nitrogen directly from crystallization droplet. Crystallization conditions are summarized in tab. 11.

**Table 11. Crystallization conditions**

Substrate	Reservoir solution	V(rhGCPIIE424 M/substrate), $\mu\text{l}$	V(reservoir solution), $\mu\text{l}$
1S	34% (v/v) pentaerythritol propoxylate PO/OH 5/4, 2%	1	2

	(w/v) PEG3350, and 100 mM Tris-HCl, pH 8.0		
<b>2S</b>	35% (v/v) pentaerythritol propoxylate PO/OH 5/4, 4% (w/v) PEG3350, and 100 mM Tris-HCl, pH 8.0	2	1
<b>3S</b>	33% (v/v) pentaerythritol propoxylate PO/OH 5/4, 2% (w/v) PEG3350, and 100 mM Tris-HCl, pH 8.0	1	2
<b>4S</b>	34% (v/v) pentaerythritol propoxylate PO/OH 5/4, 2% (w/v) PEG3350, and 100 mM Tris-HCl, pH 8.0	2	1
<b>5S</b>	33% (v/v) pentaerythritol propoxylate PO/OH 5/4, 5% (w/v) PEG3350, and 100 mM Tris-HCl, pH 8.0	1.5	1

For each rhGCPIIE424M/**1S-4S** complex, diffraction data were collected from a single crystal at 100 K using synchrotron radiation at the MX14.2 beamline (0.92 Å; BESSY II, Helmholtz-Zentrum Berlin, Berlin, Germany). Processing of datasets was performed using the XDSAPP interface by Mgr. Lucia Motlová. The data collection statistics are shown in tab. 16.

For the complex rhGCPIIE424M/**5S**, diffraction data were collected from a single crystal at 100 K using D8 Venture diffractometer (Bruker). Data were processed using XDS, XDSkappa, and XSCALE by Ing. Jan Stránský, Ph.D. The data collection statistics are shown in tab. 15.

### 3.2.6. Structure determination and refinement

Difference Fourier methods were applied to determine the structure of the rhGCPIIE424M/**1S-5S** complexes and rhGCPIIE424M/EESO complex, with ligand-free rhGCPII (PDB code 3BI1) used as a starting model. Refmac 5.8.0258<sup>186</sup> was used for calculations, refinement protocol was interspersed with manual corrections to the rhGCPIIE424M/EESO model using the program Coot 0.9<sup>187</sup>. The coordinate file and the restraints library for EESO were prepared using ACEDRG<sup>188</sup>. At the final stages of refinement, EESO was fitted into the positive electron density map. During refinement, 2179 randomly selected reflections were kept aside for cross-validation ( $R_{\text{free}}$ ). Evaluation of the final model quality was performed using the MOLPROBITY software<sup>189</sup>. Statistics are shown in tab. 16.



### 3.3. Results

GCPII is an important prostate cancer biomarker<sup>2</sup>. However, up to the date, only one direct continuous GCPII activity assay was developed, and it is not optimized for evaluation of GCPII inhibitors yet<sup>185</sup>. To develop a continuous fluorescence GCPII activity assay, small fluorescent probes (listed in tab. 5) were designed. Each probe contains a fluorophore part linked to a negatively charged amino acid (Asp – **1S**, **2S**, Glu – **3S-5S**) that is connected to the glutamate-mimicking quencher moiety. An additional linker could be present between the fluorophore and the amino acid (**2S**, **4S**, **5S**). After the cleavage of the peptide bond by GCPII, the fluorophore moiety is not quenched anymore, and a fluorescent signal can be detected.

For characterization of those probes, the following technics were used: kinetic measurements (using a microplate reader and HPLC), crystallization, diffraction data collection, solving/refining structure(s) of enzyme/substrate complexes.

#### 3.3.1. Fluorescence signal linearity – microplate readout

The substrate characterization had started from substrates **1S-4S**. Microplate fluorescence measurements were performed as described in the chapter 3.2.1 using a CLARIOstar microplate reader. According to the results of the experiments, dependence of fluorescence signal on the concentration is linear up to 25  $\mu\text{M}$ . Decrease of the fluorescence signal within one hour is negligible (data not shown). Substrate **1S** produced 8.8% of fluorescence signal of the non-quenched fluorophore, **2S** – 23.8%, **3S** – 13.1%, and **4S** – 22.7%. Based on experimental data, all substrates were confirmed to be efficiently quenched. The absence of linker in **2S** and **3S** has beneficial effect (15% and 9.6% better quenching of substrates compared to **1S** and **4S**, respectively).

Linearity and decrease in time of the fluorescent signal for substrate **5S** were measured in the same manner. The signal decrease in time was found to be negligible (data not shown). The fluorescence signal was linear up to 6.25  $\mu\text{M}$ . The substrate **5S** possesses 40.6% of the fluorescence signal of the unquenched product of its cleavage.

The quenching efficiency of substrates is summarized in tab. 12.

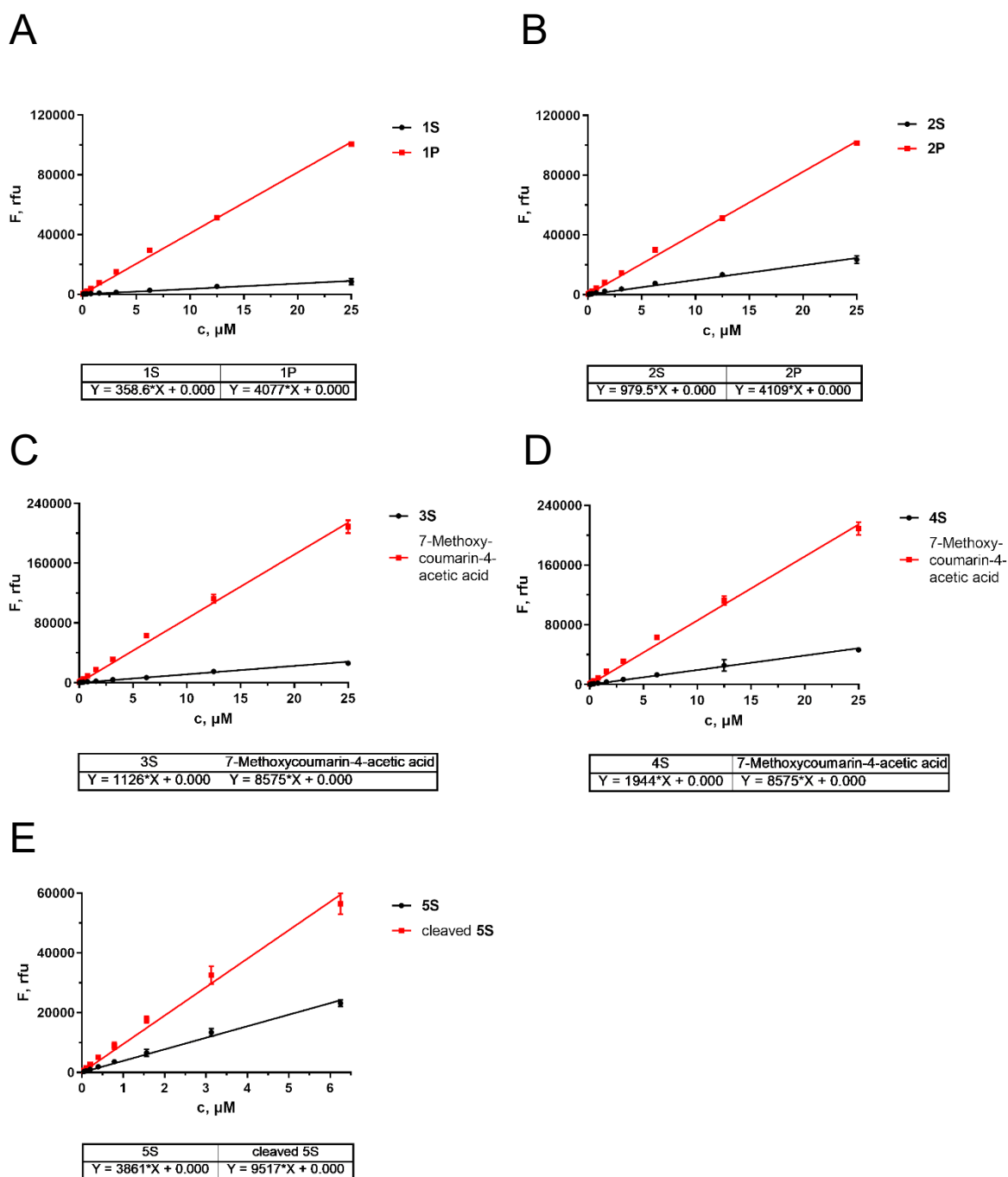


**Figure 9. Dependence of the fluorescent signal on concentration of substrates (black) and corresponding standards (red)**

Fluorescence intensity was measured using a CLARIOstar microplate reader. Equations under each graph correspond to the linear regression fits for substrates and standards, from which quenching efficiency values were calculated using formula 1. Data are shown as mean values  $\pm$  S.D.

**Table 12. Substrates' quenching efficiency**

Substrate	% quenched
1S	91.2
2S	76.2
3S	86.9
4S	77.3
5S	59.4

### 3.3.2. Kinetic measurements – microplate readout

To characterize the kinetics of substrate cleavage, parameters  $K_m$  and  $k_{cat}$  were determined as described in chapter 3.2.2 using continuous fluorescence measurement with a CLARIOstar microplate reader and analysis with GraphPad Prism software. Firstly, kinetics were measured for substrates **1S-4S**.  $K_m$  values of the substrates are comparable to those determined for NAAG by Hlouchová et al.<sup>173</sup>, but  $k_{cat}$  values are much lower. Asp-based substrates **1S-2S** showed slightly higher  $K_m$  values and 50 to 100-fold lower  $k_{cat}$  values compared to Glu-based **3S-4S**. The lowest  $K_m$  value (0.9  $\mu\text{M}$ ) was determined for the substrate **3S**. The highest  $k_{cat}$  corresponds to substrate **4S**, and  $k_{cat}$  of **3S** hydrolysis is twice lower than  $k_{cat}$  of **4S** hydrolysis.

Since comparison of substrates **1S-4S** showed that much higher  $k_{cat}$  correspond to Glu-based substrates and not Asp-based, next-generation substrates should contain glutamate as P1 amino acid moiety.

Substrate **5S** has lower  $K_m$  value than all other substrates (0.35  $\mu\text{M}$ ) and corresponding  $k_{cat}$  value comparable to one of substrate **3S**. Kinetic parameters for all substrates are summarized in tab. 13.

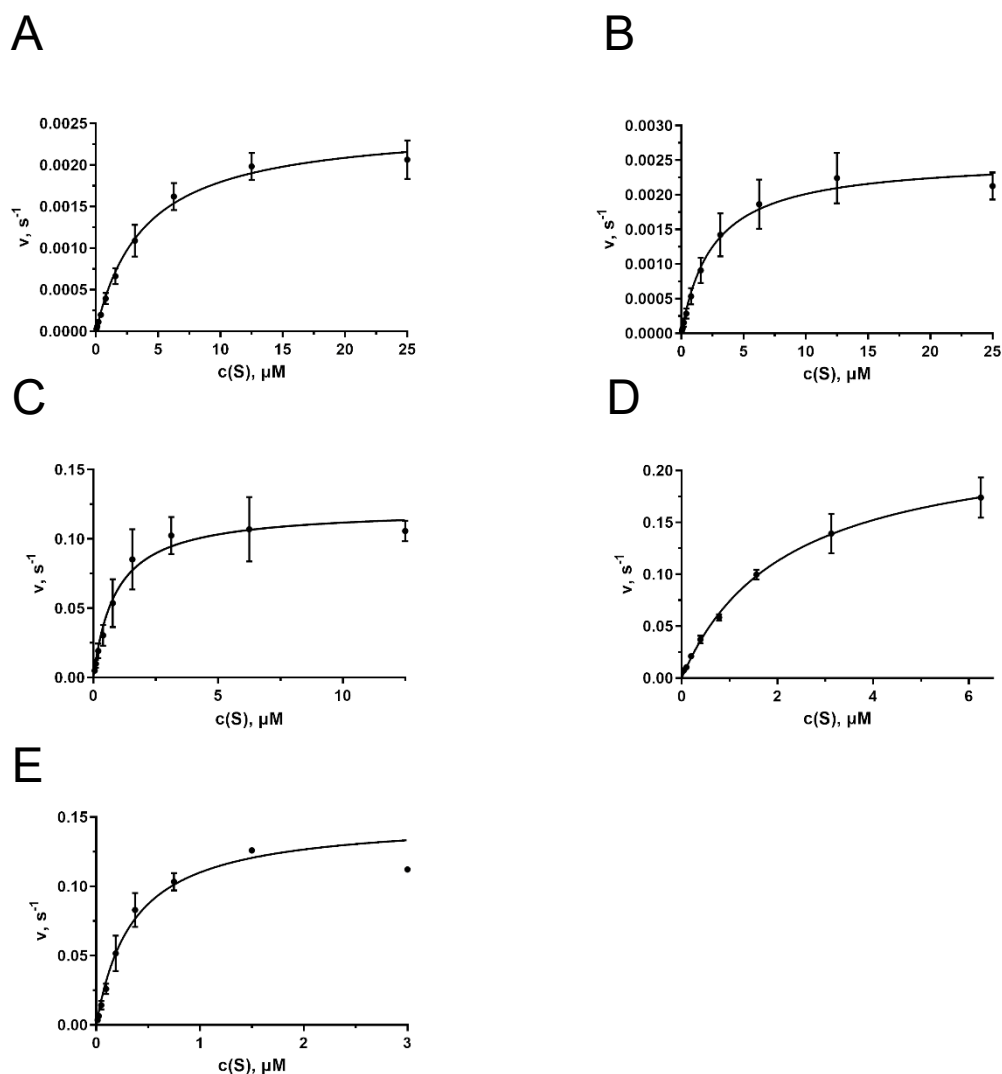


**Figure 10. Steady-state kinetics of hydrolysis of 1S (A), 2S (B), 3S (C), 4S (D), 5S (E) by GCPII – microplate readout**

Reaction progress curves were monitored with CLARIOstar microplate reader. The results for each probe are from two independent experiments, each performed in duplicate. The velocity corresponds to product formation per time unit and per active site. Velocities for each concentration point were calculated using formula 2.  $K_m$  and  $k_{cat}$  were determined from the Michaelis-Menten equation fit and are listed in tab. 13. Data are shown as mean values  $\pm$  S.D.

**Table 13. Kinetic parameters of substrate hydrolysis by GCPII**

	1S	2S	3S	4S	5S	NAAG (taken from <sup>173</sup> )
$k_{cat}, s^{-1}$	0.002490±	0.002526±	0.1217±	0.2345±	0.149±	1.1
	$8.299 \cdot 10^{-5}$	0.0001103	0.006020	0.01086	0.006354	
$K_m, \mu M$	3.872±	2.564±	0.8984±	2.162±	0.3542±	1.2
	0.3805	0.3659	0.1576	0.2335	0.04277	

### 3.3.3. Kinetic measurements – HPLC readout

To confirm the reliability of the fluorescence kinetic assay measurements, kinetic parameters for the substrate **5S** were determined using the end-point HPLC-based method as described in section 3.2.3. Resulting  $K_m$  and  $k_{cat}$  values was compared with corresponding values reported in section 3.3.2.

#### 3.3.3.1. Method development

Firstly, an optimal gradient was determined. For that, gradients 1-3 from the Table 8 were examined. Then, the method was optimized from 15-45 (gradient 2) to 20-45 (gradient 4) to improve peak separation of the substrate and the reaction product.

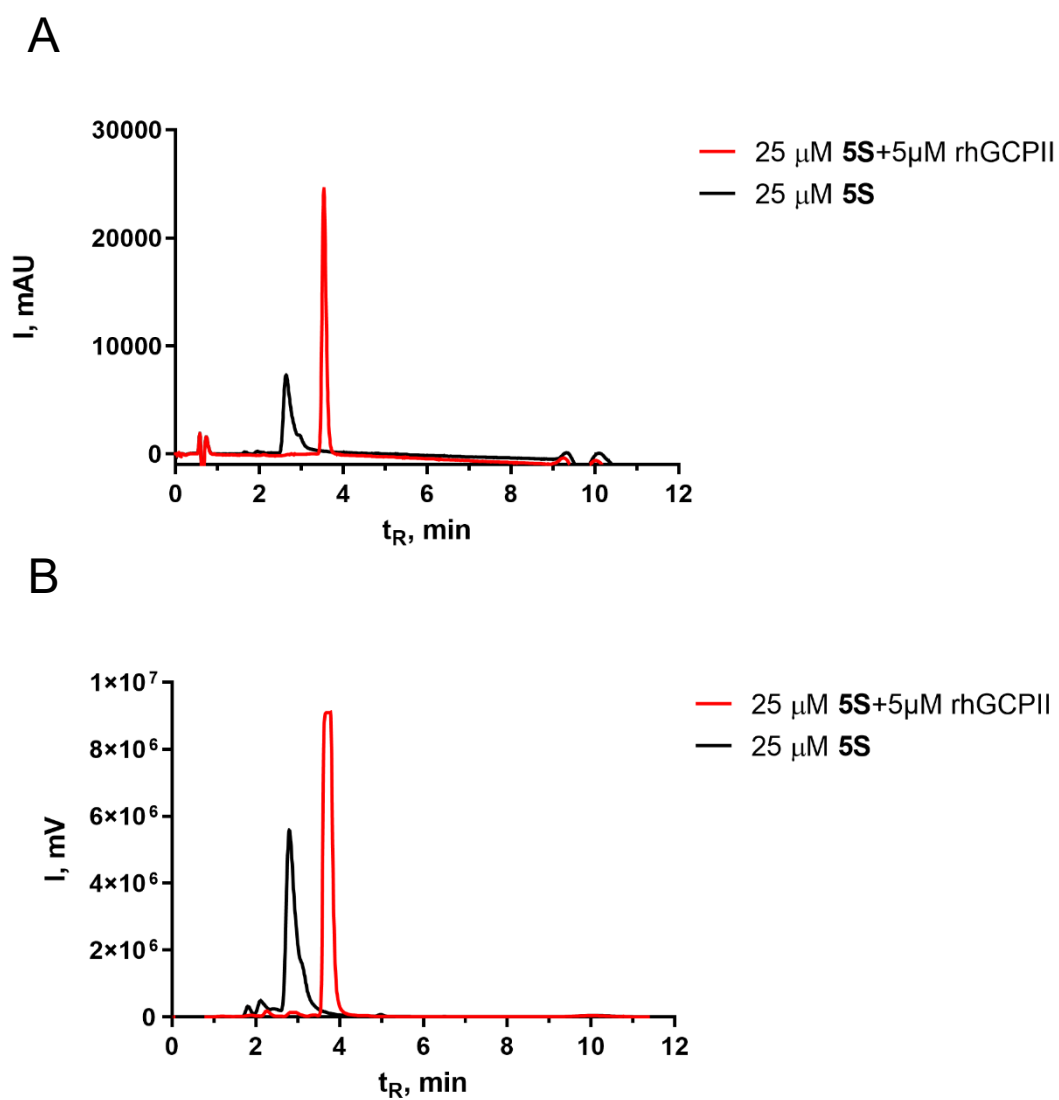


**Figure 11. HPLC chromatograms of 5S (red) and product of its cleavage (black) – absorbance (A) and fluorescence (B) detection.**

Chromatograms from Kinetex 2.6  $\mu\text{m}$  Polar C18 100  $\text{\AA}$  LC Column 50x3 mm (Phenomenex, Torrance, Canada). Eluent conditions correspond to gradient 4 (20-45) comprising solvents A (0.1 % formic acid in MilliQ water) and B (0.1 % formic acid in acetonitrile), flow rate 0.6ml/min.

### 3.3.3.2. Kinetic measurements

For substrate **5S**, kinetic parameters  $K_m$  ( $0.39 \mu\text{M}$ ) and  $k_{\text{cat}}$  ( $0.11 \text{ s}^{-1}$ ) are virtually identical to values determined with microplate fluorescence readout. On the analyzed chromatograms, one of the two present peaks corresponded to **5S** and the other to the cleavage product. Only one peak was present on chromatograms of control double-dilution series of **5S**. These data corroborate accuracy of our continuous fluorescent kinetic measurements and confirm that the increase of fluorescence signal after addition of rhGCPII is a result of enzymatic activity and not other coincidental process. Measured kinetic parameters are listed in tab 14. alongside corresponding values from section 3.3.2.

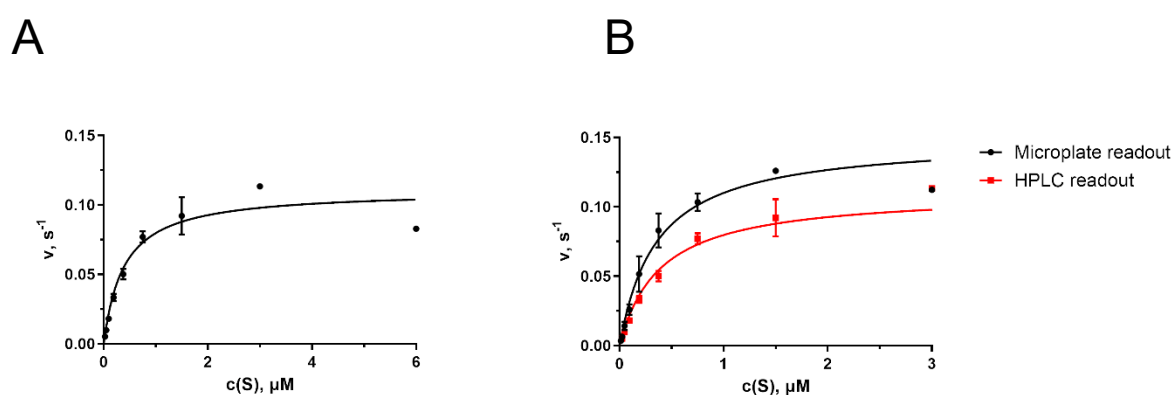


**Figure 12. Steady-state kinetics of hydrolysis of 5S by GCPII – (A) HPLC readout, (B) comparison of microplate and HPLC readouts**

- A. Reactions stopped after 30 min with 0.1% TFA were injected to Kinetex 2.6 μm Polar C18 100 Å LC Column 50x3 mm (Phenomenex, Torrance, Canada). The data are from two independent experiments, each performed in duplicate. The velocity corresponds to product formation per time unit and per active site. Velocities for each concentration point were calculated using formula 5.  $K_m$  and  $k_{\text{cat}}$  were determined from the Michaelis-Menten equation fit. Data are shown as mean values  $\pm$  S.D.
- B. HPLC and microplate readouts – comparison of data pictured at graphs from figures 12A and 10E.

**Table 14. Kinetic parameters of 5S cleavage – microplate and HPLC readout comparison**

$K_m$ , μM (HPLC readout)	$K_m$ , μM (microplate readout, section 3.3.2)	$k_{\text{cat}}$ , s <sup>-1</sup> (HPLC readout)	$k_{\text{cat}}$ , s <sup>-1</sup> (microplate readout, section 3.3.2)
$0.3867 \pm 0.07119$	$0.3542 \pm 0.04277$	$0.1105 \pm 0.005927$	$0.149 \pm 0.006354$

### 3.3.4. Determination of IC<sub>50</sub> values for T33D and DCIBzL inhibitors

Our newly developed GCPII activity assay was used to determine inhibition constants for two GCPII-specific inhibitors. For T33D, the measured IC<sub>50</sub> value (623 nM) was close to the value determined with HPLC-based assay<sup>129</sup>. For DCIBzL, the measured IC<sub>50</sub> value was approximately 40 times higher than determined with radioenzymatic assay<sup>181</sup>.

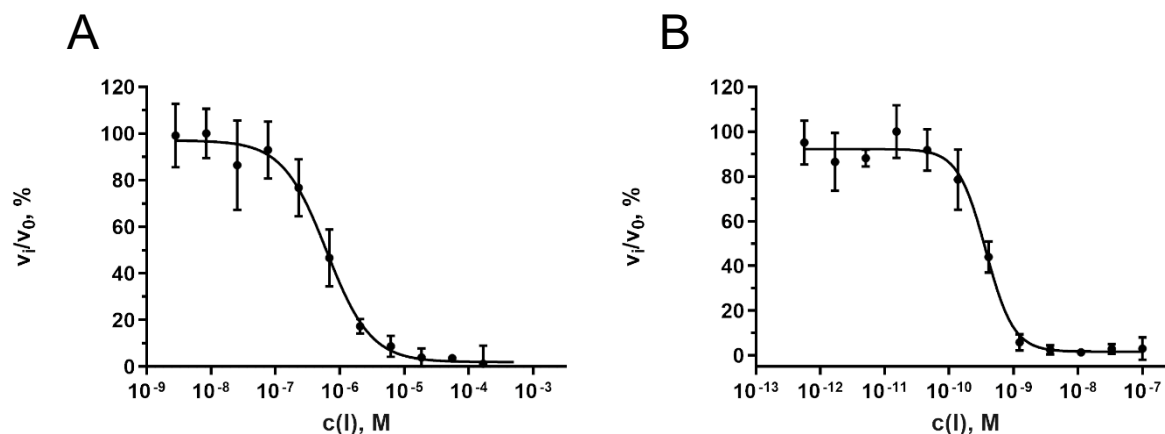


**Figure 13. Inhibition curves for competitive glutamate carboxypeptidase II (GCPII) inhibitors (A) T33D and (B) DCIBzL**

Inhibition constants of T33D and DCIBzL were determined using the newly developed continuous fluorescent GCPII activity assay and are listed in tab 15. The results for T33D are comparable to IC<sub>50</sub> value available in literature (700 nM, determined with an HPLC-based assay), while obtained inhibition constant value for DCIBzL is approximately 40 times higher than previously reported value (0.01 nM, radioenzymatic assay), since its IC<sub>50</sub> is below the limit of our assay (approximately half of the enzyme concentration, *i.e.* 0.5 nM).

**Table 14. IC<sub>50</sub> of T33D and DCIBzL**

	<b>T33D</b>	<b>DCIBzL</b>
<b>IC<sub>50</sub>, nM</b>	623	0.3705
<b>95% CI</b>	505.5 – 767.9	0.3161 – 0.4341
<b>Previously reported IC<sub>50</sub><sup>129,181</sup>, nM</b>	700	0.01

### 3.3.5. Crystallization and data collection

To characterize the binding mode and interaction pattern of probes in the active site of GCPII, complexes of substrates with rhGCPIIE424M (inactive rhGCPII mutant) were crystallized as described in section 3.2.4. Diffraction data from all complexes were successfully collected using synchrotron radiation at BESSY II or using a home-source diffractometer.



Diffraction data collection statistics are summarized in tab. 15. Structure of complexes were determined using difference Fourier methods with ligand-free rhGCPII (PDB code 3BI1) used as a starting model. However, none of the substrates' structures were completely present in the models (data not shown). The positive electron density map for each substrate was present at the active site, but was always absent for fluorophore part. Based on the fact that all substrates of interest share the same P1' and alike P1 moieties that are visible in the models, it was decided to solve and refine structure of the complex of their precursor EESO with rhGCPIIE424M.

**Table 15. Data collection statistics**

<b>Substrate</b>	<b>1S</b>	<b>2S</b>	<b>3S</b>	<b>4S</b>	<b>5S</b>
<b>Wavelength (Å)</b>	0.918	0.918	0.918	0.918	1.542
<b>Space group</b>	I222	I222	I222	I222	I222
<b>Unit-cell parameters <i>a, b, c</i> (Å)</b>	101.217 130.512 158.540	101.418 130.285 159.075	102.179 130.492 159.774	101.975 131.152 159.012	101.164 130.307 158.391
<b>Unit-cell parameters <math>\alpha, \beta, \gamma</math>, °</b>	90 90 90	90 90 90	90 90 90	90 90 90	90 90 90
<b>Resolution limits (Å)</b>	50-1.85 (1.96-1.85)	50-1.7 (1.8-1.7)	50-1.75 (1.85-1.75)	50-2.09 (2.22-2.09)	48.93-2.10 (2.15-2.10)
<b>Number of unique reflections</b>	89197 (14164)	114576 (18349)	107032 (16984)	61872 (9651)	61263 (4515)
<b>Redundancy</b>	4.436 (4.490)	4.416 (4.399)	4.427 (4.187)	4.314 (4.081)	11.93 (8.84)
<b>Completeness (%)</b>	99.5 (98.8)	99.2 (99.1)	99.1 (98.2)	97.9 (95.6)	100 (100)
<b><i>I</i>/<math>\sigma</math><i>I</i></b>	10.61 (1.37)	12.92 (1.82)	12.82 (1.47)	9.63 (1.23)	11.1 (1.1)

<b>R<sub>merge</sub></b>	0.084 (0.999)	0.07 (0.793)	0.07 (0.798)	0.131 (1.023)	0.204 (2.007)
--------------------------	------------------	-----------------	-----------------	------------------	------------------

\* Values in parenthesis are for the highest resolution shells.

### 3.3.6. Structure determination and refinement

Crystallization of the complex of EESO with rhGCPIIE424M was done prior to this thesis, as well as data collection, indexing, integration, and scaling of the dataset. All those procedures, however, were analogous to carried for rhGCPIIE424M complexes with **1S-5S**. The structure determination and refinement process is described in section 3.2.6. The final model of EESO/rhGCPIIE424M complex has resolution 1.52 Å. Refinement statistics are summarized in tab. 16.

**Table 16. Refinement statistics**

<b>Resolution limits (Å)</b>	49.29-1.517(1.557-1.517)
<b>Total number of reflections</b>	160006 (11445)
<b>Number of reflections in working set</b>	157827 (11298)
<b>Number of reflections in test set</b>	2179 (147)
<b>R/R<sub>free</sub> (%)</b>	20.25/22.26(46.6/52.1)
<b>Total number of non-H atoms</b>	6665
<b>Number of non-H protein atoms</b>	5866
<b>Number of Substrate molecules</b>	1
<b>Number of water molecules</b>	499
<b>Average B-factor (Å<sup>2</sup>)</b>	39.327
<b>&amp;Ramachandran Plot (%)</b>	
<b>Most favored</b>	98
<b>Additionally allowed</b>	2
<b>Disallowed</b>	0
<b>R.m.s. deviations: bond lengths (Å)</b>	0.008
<b>bond angles (°)</b>	1.563
<b>planarity (Å)</b>	0.009
<b>chiral centers (Å<sup>3</sup>)</b>	0.105
<b>Missing residues</b>	Lys44 – Pro54, Asp654 – Lys655

\* Values in parenthesis are for the highest resolution shells

& Structure was analyzed using the MolProbity

EESO fits into the positive electron density map in the active site of rhGCPIIE424M. Its quencher glutamate-mimicking moiety is positioned in the pharmacophore pocket and glutamate moiety occupies the S1 pocket (figure 15). Carboxylate groups of quencher interact with Asn257, Arg210, and residues of the glutarate sensor (Lys699 and Tyr700). The  $\alpha$ -carboxylate of glutamate moiety at the P1 position interacts ionically with the arginine patch in its binding conformation and forms a hydrogen bond with Asn519. The carbonyl oxygen of the scissile amide bond is polarized by the catalytic zinc (with the assistance of residues Tyr552 and His553), and the NH group of this bond plays the role of the donor in a hydrogen bond with Gly518. Distances between EESO and protein residues or water molecules that are short enough to represent ionic interactions and H-bonds are listed in tab. 17.

**Table 17. Short distances between atoms of EESO and surrounding environment**

<b>EESO atom (as denoted in figure 14)</b>	<b>rhGCPIIE424M residue/H<sub>2</sub>O</b>	<b>Distance length, Å</b>
O1	OH, Tyr700	2.54
O2	H <sub>2</sub> O	2.57
O2	NH1, Arg210	2.76
O3	H <sub>2</sub> O	3.18
O3	NZ, Lys699	3.28
O4	ND2, Asn257	2.80
O5	OH, Tyr552	2.53
O5	NE2, His553	3.13
O5	Active site H <sub>2</sub> O	2.99
O5	Catalytic Zn	2.69
O6	NH1, B/Arg536	3.15
O6	H <sub>2</sub> O	3.13

O7	NH2, Arg534	2.72
O7	ND2, Asn519	2.87
O7	H <sub>2</sub> O	2.90
O7	H <sub>2</sub> O	3.12
O8	H <sub>2</sub> O	2.62
O8	H <sub>2</sub> O	2.71
N1	O, Gly518	3.07
N3	H <sub>2</sub> O	2.91

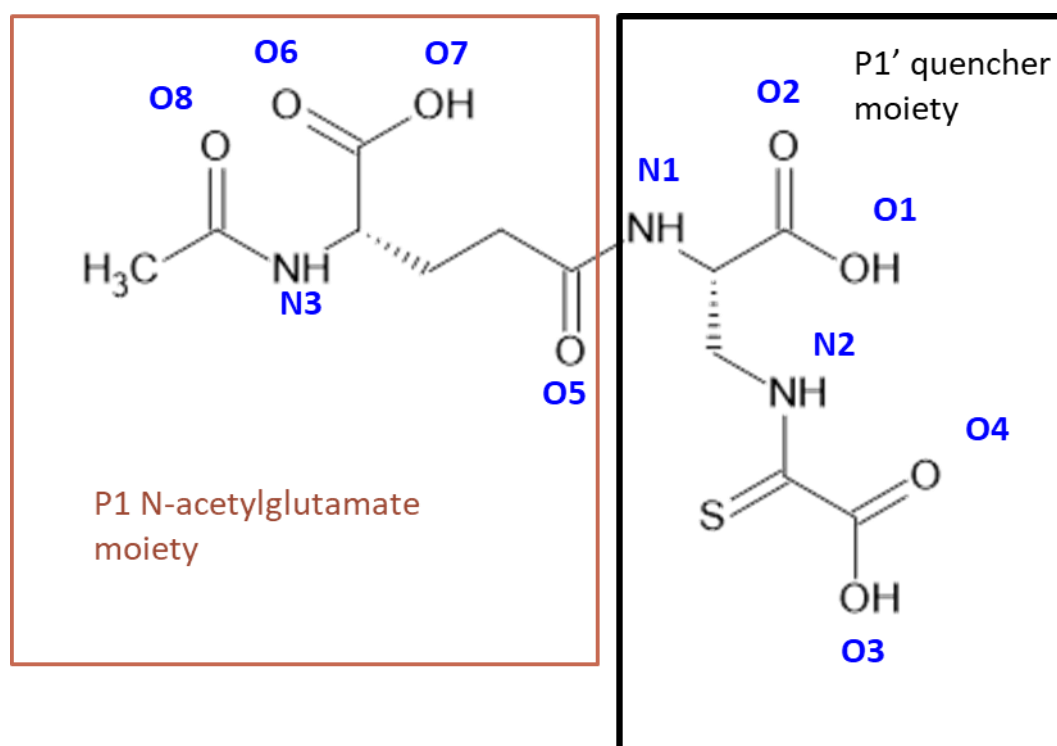


**Figure 14. Molecular formula of EESO**

EESO possesses the same thioamide-based quencher moiety as 1S-5S, which is joined to P1 glutamate N-acetylglutamate moiety with a scissile peptide bond

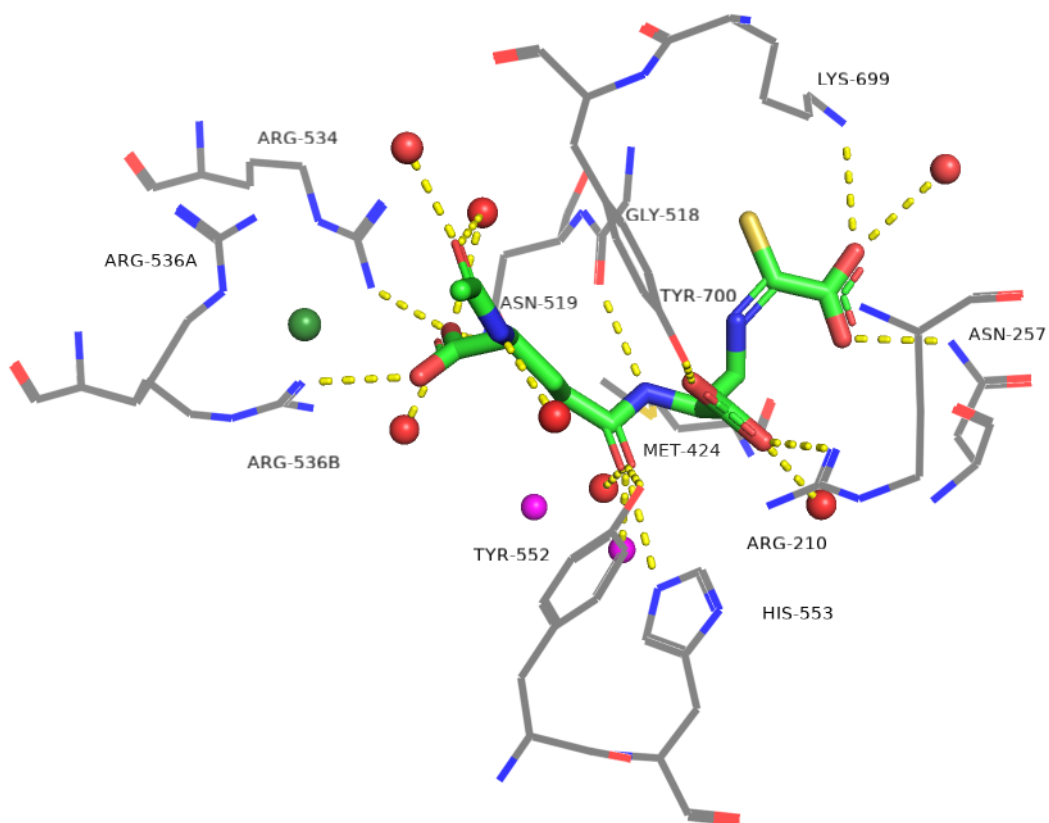


**Figure 15. EESO in the binding pocket of rhGCPIIE424M**

EESO is represented with sticks and colored by atom (green – C, blue – N, red – O, yellow – S). Residues of rhGCPIIE424M are represented with lines and colored by atom (grey – C, blue – N, red – O). Spheres represent Cl<sup>-</sup> anion (dark green), Zn<sup>2+</sup> ions (magenta) and water molecules (red). Yellow dashes represent intermolecular distances between EESO and its surroundings shorter than 3.28 Å.

### 3.4. Discussion

Glutamate carboxypeptidase II is a zinc-dependent membrane resident exopeptidase. It exhibits 95% specificity to androgen-resistant prostate carcinoma, thus being a target for its therapy and imaging<sup>2</sup>. Considering the neuroprotective effect of GCPII inhibition in the brain, GCPII is also seen as a potential target in the case of neurological diseases connected with glutamate excitotoxicity<sup>61-70</sup>. GCPII targeting agents include antibodies, antibody fragments, aptamers, and small-molecule inhibitors<sup>71</sup>. For the development of small-molecule inhibitors, there is a need for GCPII activity assay for their evaluation. Among the most used existing assays are an end-point radioenzymatic assay and an HPLC-based assay, as well as an indirect continuous Amplex Red glutamic acid assay. Up to date, no direct carboxypeptidase activity assay for inhibitors evaluation was developed.

The work described in this thesis was aimed at the development of direct fluorescence continuous GCPII activity assay. Artificial substrates (synthesized by Dr. Marat Meleshin from Martin Luther University Halle-Wittenberg, Halle, Germany) **1S-5S** (tab. 5) were designed as fluorescent probes for the assay. Each probe consists of three main parts – fluorophore, P1 amino acid (glutamate or aspartate) important for interaction with the arginine patch, and P1' quencher. The fluorophore and P1 amino acid could be connected either directly or with a linker. The quencher moiety is thioamide-based. Thioamide was shown to quench various common fluorophores (including 7-methoxycoumarin-4-yl-alanine, 5-carboxyfluorescein, Alexa Fluor 488 and BODIPY FL) through photoinduced electron transfer mechanism<sup>190,191</sup>. The main advantages of the thioamide-based quencher are its small size, which allows placing the quencher moiety at the P1' position, as well as minimal perturbation of peptide structure by thioamide substitution<sup>192</sup>. Turn-on probes with fluorophore/thioamide pairs were developed for monitoring of enzymatic activity of various proteases<sup>193</sup>. After cleavage of a substrate by the enzyme, a part with the fluorophore is detached from the quencher, and a high fluorescent signal is detected upon excitation.

Firstly, substrates **1S-4S** and respective standards were characterized. Those substrates possess a fluorophore derived from 7-Methoxy-coumarin-4-acetic acid with excitation and emission maximums in the UV part of the electromagnetic spectrum. The linear range of detection was found to be between 49 nM and 25  $\mu$ M by microplate readout. All those substrates were efficiently quenched, especially linker-lacking **1S** and **3S**.  $K_m$  and  $k_{cat}$  values describing cleavage of substrates were derived from the continuous experiments monitored with CLARIOstar. Since  $k_{cat}$  values, and, thus, maximum velocities were significantly lower for

substrates with an aspartate moiety (**1S** and **2S**), it was decided to continue the development of potential substrates only with glutamate as the P1 amino acid. Although substrates **3S** and **4S** could be potentially used for *in vitro* GCPII activity assays, the properties of their fluorophore moiety, namely emission and excitation at short wavelengths, make them impractical for fluorescent visualisation of GCPII activity *in vivo*. Thus, an attempt was made to develop substrates bearing fluorophores with red-shifted excitation/emission maximums. Before **5S**, two fluorescein-bearing substrates were examined. Those substrates, however, were highly unstable and therefore useless in practice (data not shown).

Then, **5S** with BODIPY-based fluorophore was synthesized (by Dr. Marat Meleshin as well). The linear range of detection was from 49 nM (8 nM for the product of cleavage) to 6.25  $\mu$ M.  $K_m$  and  $k_{cat}$  of this substrate's cleavage were firstly determined by continuous experiments using CLARIOstar and then confirmed with end-point HPLC experiments. The  $K_m$  value (0.35  $\mu$ M) is lower than one for a NAAG (1.2  $\mu$ M)<sup>173</sup>, the natural substrate of GCPII.  $k_{cat}$  (0.15 s<sup>-1</sup>) is comparable with one for the cleavage of **3S** (0.12 s<sup>-1</sup>). The main problem with **5S** is, unfortunately, suboptimal quenching efficiency (59.4%). However, the compound was used as a probe for our assay.

The implemented GCPII activity assay was used to determine IC<sub>50</sub> values for T33D and DCIBzL, two competitive GCPII inhibitors. For that, 0.5  $\mu$ M concentration of **5S** (approximately equal to the  $K_m$ ) and 1 nM concentration of rhGCPII were used. Measured by our assay IC<sub>50</sub> of phosphorus-based T33D (623nM) is in agreement with the value previously determined with an HPLC-based assay (700 nM)<sup>129</sup>. For urea-based DCIBzL, however, measured IC<sub>50</sub> (0.4 nM) is higher than determined with a radioenzymatic assay (0.01 nM)<sup>181</sup>. The DCIBzL is the most potent GCPII inhibitor with an extremely low IC<sub>50</sub>, which is below the limit of our assay (approximately 0.5 nM, given by half of the used enzyme concentration)<sup>140</sup>. The value obtained with our assay is the lowest possible obtainable value in used conditions. In principle, the assay limit could be pushed to lower subnanomolar concentrations by a decrease of the enzyme concentration and an increase of the assay time window.

Complexes of the inactive mutant of GCPII with each substrate were successfully crystallized, and diffraction data were collected from the single crystals either using synchrotron radiation at the MX14.2 beamline (BESSY II, Helmholtz-Zentrum Berlin, Berlin, Germany) or D8 Venture diffractometer. The positive electron density for substrates was present at the active site with the part for the quencher fitting into the pharmacophore pocket.

However, there was no positive electron density map for the fluorophore part. Based on that, the assumption about its flexible character could be made. Since the probes were not seen completely in preliminary models, it was decided to characterize the complex of their precursor EESO with the rhGCPIIE424M inactive mutant.

EESO is a peptide derived from natural GCPII substrates. It consists of N-acetyl glutamate connected to the same thioamide-based quencher moiety that is present in substrates **1S-5S**. Unlike the case of NAAG but similarly to folyl- $\gamma$ -glutamates, the peptide bond is formed between the amino group of P1' moiety and the sidechain carboxyl group of P1 amino acid instead of  $\alpha$ -carboxylate. Quencher moiety is derived from C-terminal glutamate by replacement of  $\gamma$ -carbon with nitrogen, one of the  $\gamma$ -carboxylate oxygens with sulfur, and the other with carboxyl. In the final model, the quencher moiety is present at the pharmacophore pocket as expected, even though it is slightly bulkier than glutamate (figure 15). Its carboxylates interact with the same enzyme residues as carboxylates of the C-terminal glutamate of NAAG or glutamylated folates<sup>38,170</sup>, although S1' pocket is enlarged by shift of sidechains of Asn257 (2 Å shift of N $\delta$ 2 comparing to complex with NAAG) and Lys699 (0.7 Å shift of N $\zeta$  comparing to complex with NAAG). Interactions of the  $\alpha$ -carboxylate of P1 glutamate with the arginine patch and with Asn519, as well as interactions of the scissile amide bond with active site residues, catalytic zinc, and zinc-bounded water, are similar to interactions that are present in complexes of inactive GCPII with NAAG or folate-based substrates<sup>38,170</sup>.

To this end, five substrates were analysed using biochemical and structural biology techniques. A continuous GCPII activity assay was developed with the substrate **5S** acting as a probe. The assay was used to determine IC<sub>50</sub> values for inhibitors T33D and DCIBzL. Unlike HPLC assay and radioenzymatic assay, our newly developed assay is less time-consuming and could be suitable for high throughput screening of inhibitors, however, additional validation of the assay is required as well as determination of the impact of pH, temperature, and common additives on the assay performance. In contrast with Amplex Red glutamic acid assay, there are no risks connected with the presence of additional enzymes and oxidation by H<sub>2</sub>O<sub>2</sub>. Our assay is more sensitive than HTS-suitable fluorescence polarization assay and would be more accurate for validation of inhibitors with low nanomolar and subnanomolar potency. For precise determination of IC<sub>50</sub> of more potent inhibitors, however, radioenzymatic assay is required.

By substitution of the fluorophore moiety of our substrates to near-IR fluorophores, next-generation probes that would be potentially applicable for *in vivo* GCPII activity imaging



could be generated. To improve suboptimal quenching of the **5S** substrate, modifications of quencher moiety could be conducted. For the design of the next generation of assay probes, structural information from the complex of their precursor with the inactive rhGCPII could be employed.

### 3.5. Conclusions

We developed a continuous fluorescence activity assay for glutamate carboxypeptidase II. Specifically:

- We have characterized quenching efficiency of designed fluorescent probes (substrates of GCPII).
- We have determined  $K_m$  and  $k_{cat}$  values for hydrolysis of our fluorescent probes by GCPII using a microplate reader.
- We have confirmed results of microplate reader kinetic measurements for the substrate **5S** using HPLC.
- Complexes of inactive GCPII mutant with each substrate were crystallized.
- We solved, refined and analyzed structure of the GCPIIE424M inactive mutant in complex with ESSO.

#### 4. References

1. Israeli, R. S., Powell, C. T. & Fair, W. R. Molecular Cloning of a Complementary DNA Encoding a Prostate-specific Membrane Antigen I. **1993**, 5 (1993).
2. Mhaweche-Fauceglia, P., Zhang, S., Terracciano, L., Sauter, G., Chadhuri, A., Herrmann, F. R., & Penetrante, R. Prostate-specific membrane antigen (PSMA) protein expression in normal and neoplastic tissues and its sensitivity and specificity in prostate adenocarcinoma: an immunohistochemical study using multiple tumour tissue microarray technique. *Histopathology* **50**, 472–483 (2007).
3. Vornov, J. J., Wozniak, K., Lu, M., Jackson, P., Tsukamoto, T., Wang, E., & Slusher, B. Blockade of NAALADase: A Novel Neuroprotective Strategy Based on Limiting Glutamate and Elevating NAAG. *Ann. N. Y. Acad. Sci.* **890**, 400–405 (1999).
4. O'Keefe, D. S., Su, S. L., Bacich, D. J., Horiguchi, Y., Luo, Y., Powell, C. T., Zandvliet, D., Russell, P. J., Molloy, P. L., Nowak, N. J., Shows, T. B., Mullins, C., Vonder Haar, R. A., Fair, W. R., & Heston, W. D. Mapping, genomic organization and promoter analysis of the human prostate-specific membrane antigen gene. *Biochim. Biophys. Acta* **15**.
5. Lambert, L. A. & Mitchell, S. L. Molecular Evolution of the Transferrin Receptor/Glutamate Carboxypeptidase II Family. *J. Mol. Evol.* **64**, 113–128 (2007).
6. Bzdega, T., Turi, T., Wroblewska, B., She, D., Chung, H. S., Kim, H., & Neale, J. H. Molecular Cloning of a Peptidase Against N-Acetylaspartylglutamate from a Rat Hippocampal cDNA Library. *J. Neurochem.* **69**, 2270–2277 (2002).
7. Bacich, D. J., Pinto, J. T., Tong, W. P. & Heston, W. D. W. Cloning, expression, genomic localization, and enzymatic activities of the mouse homolog of prostate-specific membrane antigen/NAALADase/folate hydrolase. *Mamm. Genome* **12**, 117–123 (2001).
8. Halsted, C. H., Ling, E. H., Luthi-Carter, R., Villanueva, J. A., Gardner, J. M., & Coyle, J. T. Folylpoly- $\gamma$ -glutamate Carboxypeptidase from Pig Jejunum. *J. Biol. Chem.* **273**, 20417–20424 (1998).

9. Rovenska, M., Hlouchova, K., Sacha, P., Mlcochova, P., Horak, V., Zamecnık, J., Barinka, C., & Konvalinka, J. Tissue expression and enzymologic characterization of human prostate specific membrane antigen and its rat and pig orthologs. *The Prostate* **68**, 171–182 (2008).
10. Aggarwal, S., Ricklis, R. M., Williams, S. A. & Denmeade, S. R. Comparative study of PSMA expression in the prostate of mouse, dog, monkey, and human. *The Prostate* **66**, 903–910 (2006).
11. Sacha, P., Zamecnık, J., Barinka, C., Hlouchova, K., Vıcha, A., Mlcochova, P., Hilgert, I., Eckschlager, T., & Konvalinka, J. Expression of glutamate carboxypeptidase II in human brain. *Neuroscience* **144**, 1361–1372 (2007).
12. Silver, D. A., Pellicer, I., Fair, W. R., Heston, W. D. & Cordon-Cardo, C. Prostate-specific membrane antigen expression in normal and malignant human tissues. *Clin. Cancer Res. Off. J. Am. Assoc. Cancer Res.* **3**, 81–85 (1997).
13. Chang, S. S., Reuter, V. E., Heston, W. D., Bander, N. H., Grauer, L. S., & Gaudin, P. B.. Five different anti-prostate-specific membrane antigen (PSMA) antibodies confirm PSMA expression in tumor-associated neovasculature. *Cancer Res.* **59**, 3192–3198 (1999).
14. Kinoshita, Y., Kuratsukuri, K., Landas, S., Imaida, K., Rovito, P. M., Jr, Wang, C. Y., & Haas, G. P. Expression of prostate-specific membrane antigen in normal and malignant human tissues. *World J. Surg.* **30**, 628–636 (2006).
15. Sokoloff, R. L., Norton, K. C., Gasior, C. L., Marker, K. M. & Grauer, L. S. A dual-monoclonal sandwich assay for prostate-specific membrane antigen: levels in tissues, seminal fluid and urine. *The Prostate* **43**, 150–157 (2000).
16. Troyer, J. K., Beckett, M. L. & Wright, G. L. J. Detection and characterization of the prostate-specific membrane antigen (PSMA) in tissue extracts and body fluids. *Int. J. Cancer* **62**, 552–558 (1995).

17. Robinson, M. B., Blakely, R. D., Couto, R. & Coyle, J. T. Hydrolysis of the brain dipeptide N-acetyl-L-aspartyl-L-glutamate. Identification and characterization of a novel N-acetylated alpha-linked acidic dipeptidase activity from rat brain. *J Biol Chem.* **262**, 14498-14506 (1987).
18. Curatolo, A., D Arcangelo, P., Lino, A. & Brancati, A. Distribution Of N-acetyl-aspartic And N-acetyl-aspartyl-glutamic Acids In Nervous Tissue. *J. Neurochem.* **12**, 339–342 (1965).
19. Pouwels, P. J. & Frahm, J. Differential distribution of NAA and NAAG in human brain as determined by quantitative localized proton MRS. *NMR Biomed.* **10**, 73–78 (1997).
20. Williamson, L. C. & Neale, J. H. Ultrastructural localization of N-acetylaspartylglutamate in synaptic vesicles of retinal neurons. *Brain Res.* **456**, 375–381 (1988).
21. Renno, W. M., Lee, J. H. & Beitz, A. J. Light and electron microscopic immunohistochemical localization of N-acetylaspartylglutamate (NAAG) in the olivocerebellar pathway of the rat. *Synap. N. Y. N* **26**, 140–154 (1997).
22. Pittaluga, A., Barbeito, L., Serval, V., Godeheu, G., Artaud, F., Glowinski, J., & Chéramy, A. Depolarization-evoked release of N-acetyl-L-aspartyl-L-glutamate from rat brain synaptosomes. *Eur. J. Pharmacol.* **158**, 263–266 (1988).
23. Zollinger, M., Amsler, U., Do, K. Q., Streit, P. & Cuénod, M. Release of N-acetylaspartylglutamate on depolarization of rat brain slices. *J. Neurochem.* **51**, 1919–1923 (1988).
24. Zollinger M, Brauchli-Theotokis J, Gutteck-Amsler U, Do KQ, Streit P, Cuénod M. Release of N-acetylaspartylglutamate from slices of rat cerebellum, striatum, and spinal cord, and the effect of climbing fiber deprivation. *J. Neurochem.* **63**, 1133–1142 (1994).
25. Khacho, P., Wang, B., Ahlskog, N., Hristova, E. & Bergeron, R. Differential effects of N-acetyl-aspartyl-glutamate on synaptic and extrasynaptic NMDA receptors are subunit- and

- pH-dependent in the CA1 region of the mouse hippocampus. *Neurobiol. Dis.* **82**, 580–592 (2015).
26. Wroblewska, B., Santi, M. R. & Neale, J. H. N-acetylaspartylglutamate activates cyclic AMP-coupled metabotropic glutamate receptors in cerebellar astrocytes. *Glia* **24**, 172–179 (1998).
27. Wroblewska, B., Wegorzewska, I. N., Bzdega, T., Olszewski, R. T. & Neale, J. H. Differential negative coupling of type 3 metabotropic glutamate receptor to cyclic GMP levels in neurons and astrocytes. *J. Neurochem.* **96**, 1071–1077 (2006).
28. Bruno, V., Battaglia, G., Casabona, G., Copani, A., Caciagli, F., & Nicoletti, F. Neuroprotection by glial metabotropic glutamate receptors is mediated by transforming growth factor-beta. *J. Neurosci. Off. J. Soc. Neurosci.* **18**, 9594–9600 (1998).
29. Xi, Z.-X., Baker, D. A., Shen, H., Carson, D. S. & Kalivas, P. W. Group II metabotropic glutamate receptors modulate extracellular glutamate in the nucleus accumbens. *J. Pharmacol. Exp. Ther.* **300**, 162–171 (2002).
30. Sánchez-Prieto, J., Budd, D. C., Herrero, I., Vázquez, E. & Nicholls, D. G. Presynaptic receptors and the control of glutamate exocytosis. *Trends Neurosci.* **19**, 235–239 (1996).
31. Halsted, C. H., Ling, E. H., Luthi-Carter, R., Villanueva, J. A., Gardner, J. M., & Coyle, J. T. Folylpoly-gamma-glutamate carboxypeptidase from pig jejunum. Molecular characterization and relation to glutamate carboxypeptidase II. *J. Biol. Chem.* **273**, 20417–20424 (1998).
32. Halsted, C. H. The intestinal absorption of dietary folates in health and disease. *J. Am. Coll. Nutr.* **8**, 650–658 (1989).
33. Herbert, V. Biochemical and hematologic lesions in folic acid deficiency. *Am. J. Clin. Nutr.* **20**, 562–572 (1967).

34. Mills, J. L., McPartlin, J. M., Kirke, P. N., Lee, Y. J., Conley, M. R., Weir, D. G., & Scott, J. M. Homocysteine metabolism in pregnancies complicated by neural-tube defects. *Lancet Lond. Engl.* **345**, 149–151 (1995).
35. Boushey, C. J., Beresford, S. A., Omenn, G. S. & Motulsky, A. G. A quantitative assessment of plasma homocysteine as a risk factor for vascular disease. Probable benefits of increasing folic acid intakes. *JAMA* **274**, 1049–1057 (1995).
36. Ma, J., Stampfer, M. J., Giovannucci, E., Artigas, C., Hunter, D. J., Fuchs, C., Willett, W. C., Selhub, J., Hennekens, C. H., & Rozen, R. Methylene tetrahydrofolate reductase polymorphism, dietary interactions, and risk of colorectal cancer. *Cancer Res.* **57**, 1098–1102 (1997).
37. Devlin, A. M., Ling, E. H., Peerson, J. M., Fernando, S., Clarke, R., Smith, A. D., & Halsted, C. H. Glutamate carboxypeptidase II: a polymorphism associated with lower levels of serum folate and hyperhomocysteinemia. *Hum. Mol. Genet.* **9**, 2837–2844 (2000).
38. Navrátil, M., Ptáček, J., Šácha, P., Starková, J., Lubkowski, J., Bařinka, C., & Konvalinka, J. Structural and biochemical characterization of the folyl-poly- $\gamma$ -l-glutamate hydrolyzing activity of human glutamate carboxypeptidase II. *FEBS J.* **281**, 3228–3242 (2014).
39. Halsted, C. H., Wong, D. H., Peerson, J. M., Warden, C. H., Refsum, H., Smith, A. D., Nygård, O. K., Ueland, P. M., Vollset, S. E., & Tell, G. S. Relations of glutamate carboxypeptidase II (GCPII) polymorphisms to folate and homocysteine concentrations and to scores of cognition, anxiety, and depression in a homogeneous Norwegian population: the Hordaland Homocysteine Study. *Am. J. Clin. Nutr.* **86**, 514–521 (2007).
40. Vargas-Martinez, C., Ordovas, J. M., Wilson, P. W. & Selhub, J. The glutamate carboxypeptidase gene II (C>T) polymorphism does not affect folate status in the Framingham Offspring cohort. *J. Nutr.* **132**, 1176–1179 (2002).

41. Devlin, A. M., Clarke, R., Birks, J., Evans, J. G. & Halsted, C. H. Interactions among polymorphisms in folate-metabolizing genes and serum total homocysteine concentrations in a healthy elderly population. *Am. J. Clin. Nutr.* **83**, 708–713 (2006).
42. Dumas, F., Gala, J. L., Berteau, P., Brasseur, F., Eschwège, P., Paradis, V., Lacour, B., Philippe, M., & Loric, S. Molecular expression of PSMA mRNA and protein in primary renal tumors. *Int. J. Cancer* **80**, 799–803 (1999).
43. Gala, J. L., Loric, S., Guiot, Y., Denmeade, S. R., Gady, A., Brasseur, F., Heusterspreute, M., Eschwège, P., De Nayer, P., Van Cangh, P., & Tombal, B. Expression of prostate-specific membrane antigen in transitional cell carcinoma of the bladder: prognostic value? *Clin. Cancer Res. Off. J. Am. Assoc. Cancer Res.* **6**, 4049–4054 (2000).
44. Wang, W., Tavora, F., Sharma, R., Eisenberger, M. & Netto, G. J. PSMA expression in Schwannoma: a potential clinical mimicker of metastatic prostate carcinoma. *Urol. Oncol.* **27**, 525–528 (2009).
45. Ananias, H. J. K., van den Heuvel, M. C., Helfrich, W. & de Jong, I. J. Expression of the gastrin-releasing peptide receptor, the prostate stem cell antigen and the prostate-specific membrane antigen in lymph node and bone metastases of prostate cancer. *The Prostate* **69**, 1101–1108 (2009).
46. Liu, H., Moy, P., Kim, S., Xia, Y., Rajasekaran, A., Navarro, V., Knudsen, B., & Bander, N. H. Monoclonal antibodies to the extracellular domain of prostate-specific membrane antigen also react with tumor vascular endothelium. *Cancer Res.* **57**, 3629–3634 (1997).
47. Gordon, I. O., Tretiakova, M. S., Noffsinger, A. E., Hart, J., Reuter, V. E., & Al-Ahmadie, H. A. Prostate-specific membrane antigen expression in regeneration and repair. *Mod. Pathol.* **21**, 1421–1427 (2008).



48. Yao, V. & Bacich, D. J. Prostate specific membrane antigen (PSMA) expression gives prostate cancer cells a growth advantage in a physiologically relevant folate environment in vitro. *Prostate*, **66**, 867–75 (2006).
49. Conway, R. E., Petrovic, N., Li, Z., Heston, W., Wu, D., & Shapiro, L. H. Prostate-Specific Membrane Antigen Regulates Angiogenesis by Modulating Integrin Signal Transduction. *Mol. Cell. Biol.* **26**, 5310–5324 (2006).
50. Colombatti, M., Grasso, S., Porzia, A., Fracasso, G., Scupoli, M. T., Cingarlini, S., Poffe, O., Naim, H. Y., Heine, M., Tridente, G., Mainiero, F., & Ramarli, D. The Prostate Specific Membrane Antigen Regulates the Expression of IL-6 and CCL5 in Prostate Tumour Cells by Activating the MAPK Pathways. *PLoS ONE* **4**, 11 (2009).
51. Lapidus, R. G., Tiffany, C. W., Isaacs, J. T. & Slusher, B. S. Prostate-specific membrane antigen (PSMA) enzyme activity is elevated in prostate cancer cells. *The Prostate* **45**, 350–354 (2000).
52. Yao, V., Berkman, C. E., Choi, J. K., O’Keefe, D. S. & Bacich, D. J. Expression of prostate-specific membrane antigen (PSMA), increases cell folate uptake and proliferation and suggests a novel role for PSMA in the uptake of the non-polyglutamated folate, folic acid: PSMA Increases Folate Uptake and Proliferation. *The Prostate* **70**, 305–316 (2010).
53. Nguyen, T., Kirsch, B. J., Asaka, R., Nabi, K., Quinones, A., Tan, J., Antonio, M. J., Camelo, F., Li, T., Nguyen, S., Hoang, G., Nguyen, K., Udupa, S., Sazeides, C., Shen, Y. A., Elgogary, A., Reyes, J., Zhao, L., Kleensang, A., Chaichana, K. L., ... Le, A. Uncovering the Role of N-Acetyl-Aspartyl-Glutamate as a Glutamate Reservoir in Cancer. *Cell Rep.* **27**, 491-501.e6 (2019).
54. Kaittanis, C., Andreou, C., Hieronymus, H., Mao, N., Foss, C. A., Eiber, M., Weirich, G., Panchal, P., Gopalan, A., Zurita, J., Achilefu, S., Chiosis, G., Ponomarev, V., Schwaiger, M., Carver, B. S., Pomper, M. G., & Grimm, J. Prostate-specific membrane antigen

- cleavage of vitamin B9 stimulates oncogenic signaling through metabotropic glutamate receptors. *J. Exp. Med.* **215**, 159–175 (2018).
55. Conway, R. E., Rojas, C., Alt, J., Nováková, Z., Richardson, S. M., Rodrick, T. C., Fuentes, J. L., Richardson, N. H., Attalla, J., Stewart, S., Fahmy, B., Barinka, C., Ghosh, M., Shapiro, L. H., & Slusher, B. S. Prostate-specific membrane antigen (PSMA)-mediated laminin proteolysis generates a pro-angiogenic peptide. *Angiogenesis* **19**, 487–500 (2016).
56. Rajasekaran, S. A., Christiansen, J. J., Schmid, I., Oshima, E., Ryazantsev, S., Sakamoto, K., Weinstein, J., Rao, N. P., & Rajasekaran, A. K. Prostate-specific membrane antigen associates with anaphase-promoting complex and induces chromosomal instability. *Mol. Cancer Ther.* **7**, 2142–2151 (2008).
57. Mlcochová, P., Barinka, C., Tykvart, J., Sácha, P. & Konvalinka, J. Prostate-specific membrane antigen and its truncated form PSM'. *The Prostate* **69**, 471–479 (2009).
58. Bostwick, D. G., Pacelli, A., Blute, M., Roche, P. & Murphy, G. P. Prostate specific membrane antigen expression in prostatic intraepithelial neoplasia and adenocarcinoma: a study of 184 cases. *Cancer* **82**, 2256–2261 (1998).
59. Burger, M. J., Tebay, M. A., Keith, P. A., Samaratunga, H. M., Clements, J., Lavin, M. F., & Gardiner, R. A. Expression analysis of delta-catenin and prostate-specific membrane antigen: their potential as diagnostic markers for prostate cancer. *Int. J. Cancer* **100**, 228–237 (2002).
60. Chang, S. S., O'Keefe, D. S., Bacich, D. J., Reuter, V. E., Heston, W. D., & Gaudin, P. B. Prostate-specific membrane antigen is produced in tumor-associated neovasculature. *Clin. Cancer Res. Off. J. Am. Assoc. Cancer Res.* **5**, 2674–2681 (1999).
61. Olszewski, R. T., Janczura, K. J., Bzdega, T., Der, E. K., Venzor, F., O'Rourke, B., Hark, T. J., Craddock, K. E., Balasubramanian, S., Moussa, C., & Neale, J. H. NAAG Peptidase

- Inhibitors Act via mGluR3: Animal Models of Memory, Alzheimer's, and Ethanol Intoxication. *Neurochem. Res.* **42**, 2646–2657 (2017).
62. Zhong, C., Zhao, X., Sarva, J., Kozikowski, A., Neale, J. H., & Lyeth, B. G. NAAG peptidase inhibitor reduces acute neuronal degeneration and astrocyte damage following lateral fluid percussion TBI in rats. *J. Neurotrauma* **22**, 266–276 (2005).
63. Slusher, B. S., Vornov, J. J., Thomas, A. G., Hurn, P. D., Harukuni, I., Bhardwaj, A., Traystman, R. J., Robinson, M. B., Britton, P., Lu, X. C., Tortella, F. C., Wozniak, K. M., Yudkoff, M., Potter, B. M., & Jackson, P. F. Selective inhibition of NAALADase, which converts NAAG to glutamate, reduces ischemic brain injury. *Nat. Med.* **5**, 1396–1402 (1999).
64. Ghadge, G. D., Slusher, B. S., Bodner, A., Canto, M. D., Wozniak, K., Thomas, A. G., Rojas, C., Tsukamoto, T., Majer, P., Miller, R. J., Monti, A. L., & Roos, R. P. Glutamate carboxypeptidase II inhibition protects motor neurons from death in familial amyotrophic lateral sclerosis models. *Proc. Natl. Acad. Sci. U. S. A.* **100**, 9554–9559 (2003).
65. Rahn, K. A., Watkins, C. C., Alt, J., Rais, R., Stathis, M., Grishkan, I., Crainiceau, C. M., Pomper, M. G., Rojas, C., Pletnikov, M. V., Calabresi, P. A., Brandt, J., Barker, P. B., Slusher, B. S., & Kaplin, A. I. Inhibition of Glutamate Carboxypeptidase II (GCPII) activity as a treatment for cognitive impairment in multiple sclerosis. *Proc. Natl. Acad. Sci.* **109**, 20101–20106 (2012).
66. Yamamoto, T., Saito, O., Aoe, T., Bartolozzi, A., Sarva, J., Zhou, J., Kozikowski, A., Wroblewska, B., Bzdega, T. and Neale, J.H. Local administration of N-acetylaspartylglutamate (NAAG) peptidase inhibitors is analgesic in peripheral pain in rats. *Eur. J. Neurosci.* **25**, 147–158 (2007).

67. Chen, S.-R., Wozniak, K. M., Slusher, B. S. & Pan, H.-L. Effect of 2-(phosphono-methyl)-pentanedioic acid on allodynia and afferent ectopic discharges in a rat model of neuropathic pain. *J. Pharmacol. Exp. Ther.* **300**, 662–667 (2002).
68. Carozzi, V. A., Chiorazzi, A., Canta, A., Lapidus, R. G., Slusher, B. S., Wozniak, K. M., & Cavaletti, G. Glutamate carboxypeptidase inhibition reduces the severity of chemotherapy-induced peripheral neurotoxicity in rat. *Neurotox. Res.* **17**, 380–391 (2010).
69. Witkin, J. M., Gasior, M., Schad, C., Zapata, A., Shippenberg, T., Hartman, T., & Slusher, B. S. NAALADase (GCP II) inhibition prevents cocaine-kindled seizures. *Neuropharmacology* **43**, 348–356 (2002).
70. Olszewski, R. T., Wegorzewska, M. M., Monteiro, A. C., Krolikowski, K. A., Zhou, J., Kozikowski, A. P., Long, K., Mastropaolo, J., Deutsch, S. I., & Neale, J. H. Phencyclidine and dizocilpine induced behaviors reduced by N-acetylaspartylglutamate peptidase inhibition via metabotropic glutamate receptors. *Biol. Psychiatry* **63**, 86–91 (2008).
71. Foss, C. A., Mease, R. C., Cho, S. Y., Kim, H. J. & Pomper, M. G. GCPII imaging and cancer. *Curr. Med. Chem.* **19**, 1346–1359 (2012).
72. Chen, Y., Dhara, S., Banerjee, S. R., Byun, Y., Pullambhatla, M., Mease, R. C., & Pomper, M. G. A low molecular weight PSMA-based fluorescent imaging agent for cancer. *Biochem. Biophys. Res. Commun.* **390**, 624–629 (2009).
73. Evans, J. C., Malhotra, M., Cryan, J. F. & O’Driscoll, C. M. The therapeutic and diagnostic potential of the prostate specific membrane antigen/glutamate carboxypeptidase II (PSMA/GCPII) in cancer and neurological disease. *Br. J. Pharmacol.* **173**, 3041–3079 (2016).
74. Horoszewicz, J. S., Kawinski, E. & Murphy, G. P. Monoclonal antibodies to a new antigenic marker in epithelial prostatic cells and serum of prostatic cancer patients. *Anticancer Res.* **7**, 927–935 (1987).

75. Murphy, G. P., Maguire, R. T., Rogers, B., Partin, A. W., Nelp, W. B., Troychak, M. J., Ragde, H., Kenny, G. M., Barren, R. J., 3rd, Bowes, V. A., Gregorakis, A. K., Holmes, E. H., & Boynton, A. L. Comparison of serum PSMA, PSA levels with results of Cytogen-356 ProstaScint scanning in prostatic cancer patients. *The Prostate* **33**, 281–285 (1997).
76. Ellis, R. J., Kaminsky, D. A., Zhou, E. H., Fu, P., Chen, W. D., Brelin, A., Faulhaber, P. F., & Bodner, D. Ten-year outcomes: the clinical utility of single photon emission computed tomography/computed tomography capromab pendetide (Prostascint) in a cohort diagnosed with localized prostate cancer. *Int. J. Radiat. Oncol. Biol. Phys.* **81**, 29–34 (2011).
77. Troyer, J. K., Feng, Q., Beckett, M. L. & Wright, G. L. J. Biochemical characterization and mapping of the 7E11-C5.3 epitope of the prostate-specific membrane antigen. *Urol. Oncol.* **1**, 29–37 (1995).
78. Mease, R. C. Radionuclide based imaging of prostate cancer. *Curr. Top. Med. Chem.* **10**, 1600–1616 (2010).
79. Bander, N. H., Nanus, D. M., Milowsky, M. I., Kostakoglu, L., Vallabahajosula, S., & Goldsmith, S. J. Targeted systemic therapy of prostate cancer with a monoclonal antibody to prostate-specific membrane antigen. *Semin. Oncol.* **30**, 667–676 (2003).
80. Deb, N., Goris, M., Trisler, K., Fowler, S., Saal, J., Ning, S., Becker, M., Marquez, C., & Knox, S. Treatment of hormone-refractory prostate cancer with 90Y-CYT-356 monoclonal antibody. *Clin. Cancer Res. Off. J. Am. Assoc. Cancer Res.* **2**, 1289–1297 (1996).
81. Nanus, D. M., Milowsky, M. I., Kostakoglu, L., Smith-Jones, P. M., Vallabahajosula, S., Goldsmith, S. J., & Bander, N. H. Clinical use of monoclonal antibody HuJ591 therapy: targeting prostate specific membrane antigen. *J. Urol.* **170**, S84-S89 (2003).
82. Evans, M., Ulmert, D., Holland, J., Doran, M., Spratt, D., Sawyers, C., & Lewis, J. Imaging Androgen Receptor Signaling in Prostate Cancer with PET. *J. Nucl. Med.* **56**, 175 (2015).

83. Smith-Jones, P. M., Vallabhajosula, S., Navarro, V., Bastidas, D., Goldsmith, S. J., & Bander, N. H. Radiolabeled monoclonal antibodies specific to the extracellular domain of prostate-specific membrane antigen: preclinical studies in nude mice bearing LNCaP human prostate tumor. *J. Nucl. Med. Off. Publ. Soc. Nucl. Med.* **44**, 610–617 (2003).
84. Bander, N. H., Trabulsi, E. J., Kostakoglu, L., Yao, D., Vallabhajosula, S., Smith-Jones, P., Joyce, M. A., Milowsky, M., Nanus, D. M., & Goldsmith, S. J. Targeting metastatic prostate cancer with radiolabeled monoclonal antibody J591 to the extracellular domain of prostate specific membrane antigen. *J. Urol.* **170**, 1717–1721 (2003).
85. Holland, J. P., Divilov, V., Bander, N. H., Smith-Jones, P. M., Larson, S. M., & Lewis, J. S. <sup>89</sup>Zr-DFO-J591 for ImmunoPET of Prostate-Specific Membrane Antigen Expression In Vivo. *J. Nucl. Med.* **51**, 1293 (2010).
86. Smith-Jones, P. M., Vallabhajosula, S., Goldsmith, S. J., Navarro, V., Hunter, C. J., Bastidas, D., & Bander, N. H. In vitro characterization of radiolabeled monoclonal antibodies specific for the extracellular domain of prostate-specific membrane antigen. *Cancer Res.* **60**, 5237–5243 (2000).
87. Li, Y., Tian, Z., Rizvi, S. M. A., Bander, N. H. & Allen, B. J. In vitro and preclinical targeted alpha therapy of human prostate cancer with Bi-213 labeled J591 antibody against the prostate specific membrane antigen. *Prostate Cancer Prostatic Dis.* **5**, 36–46 (2002).
88. McDevitt, M. R., Ma, D., Lai, L. T., Simon, J., Borchartd, P., Frank, R. K., Wu, K., Pellegrini, V., Curcio, M. J., Miederer, M., Bander, N. H., & Scheinberg, D. A. Tumor therapy with targeted atomic nanogenerators. *Science* **294**, 1537–1540 (2001).
89. Vallabhajosula, S., Kuji, I., Hamacher, K. A., Konishi, S., Kostakoglu, L., Kothari, P. A., Milowski, M. I., Nanus, D. M., Bander, N. H., & Goldsmith, S. J. Pharmacokinetics and biodistribution of <sup>111</sup>In- and <sup>177</sup>Lu-labeled J591 antibody specific for prostate-specific

- membrane antigen: prediction of  $^{90}\text{Y}$ -J591 radiation dosimetry based on  $^{111}\text{In}$  or  $^{177}\text{Lu}$ ? *J. Nucl. Med. Off. Publ. Soc. Nucl. Med.* **46**, 634–641 (2005).
90. Nakajima, T., Mitsunaga, M., Bander, N. H., Heston, W. D., Choyke, P. L., & Kobayashi, H. Targeted, activatable, in vivo fluorescence imaging of prostate-specific membrane antigen (PSMA) positive tumors using the quenched humanized J591 antibody-indocyanine green (ICG) conjugate. *Bioconjug. Chem.* **22**, 1700–1705 (2011).
91. Fracasso, G., Bellisola, G., Cingarlini, S., Castelletti, D., Prayer-Galetti, T., Pagano, F., Tridente, G., & Colombatti, M. Anti-tumor effects of toxins targeted to the prostate specific membrane antigen. *The Prostate* **53**, 9–23 (2002).
92. Russell, P. J., Hewish, D., Carter, T., Sterling-Levis, K., Ow, K., Hattarki, M., Doughty, L., Guthrie, R., Shapira, D., Molloy, P. L., Werkmeister, J. A., & Kortt, A. A. Cytotoxic properties of immunoconjugates containing melittin-like peptide 101 against prostate cancer: in vitro and in vivo studies. *Cancer Immunol. Immunother. CII* **53**, 411–421 (2004).
93. Henry, M. D., Wen, S., Silva, M. D., Chandra, S., Milton, M., & Worland, P. J. A Prostate-Specific Membrane Antigen-Targeted Monoclonal Antibody–Chemotherapeutic Conjugate Designed for the Treatment of Prostate Cancer. *Cancer Res.* **64**, 7995 (2004).
94. Milowsky, M. I., Galsky, M. D., Morris, M. J., Crona, D. J., George, D. J., Dreicer, R., Tse, K., Petruck, J., Webb, I. J., Bander, N. H., Nanus, D. M., & Scher, H. I. Phase 1/2 multiple ascending dose trial of the prostate-specific membrane antigen-targeted antibody drug conjugate MLN2704 in metastatic castration-resistant prostate cancer. *Urol. Oncol.* **34**, 530.e15-530.e21 (2016).
95. Wolf, P., Freudenberg, N., Bühler, P., Alt, K., Schultze-Seemann, W., Wetterauer, U., & Elsässer-Beile, U. Three conformational antibodies specific for different PSMA epitopes are promising diagnostic and therapeutic tools for prostate cancer. *The Prostate* **70**, 562–569 (2010).

96. Alt, K., Wiehr, S., Ehrlichmann, W., Reischl, G., Wolf, P., Pichler, B. J., Elsässer-Beile, U., & Bühler, P. High-resolution animal PET imaging of prostate cancer xenografts with three different  $^{64}\text{Cu}$ -labeled antibodies against native cell-adherent PSMA. *The Prostate* **70**, 1413–1421 (2010).
97. Nováková, Z., Foss, C. A., Copeland, B. T., Morath, V., Baranová, P., Havlínová, B., Skerra, A., Pomper, M. G., & Barinka, C. Novel Monoclonal Antibodies Recognizing Human Prostate-Specific Membrane Antigen (PSMA) as Research and Theranostic Tools. *The Prostate* **77**, 749–764 (2017).
98. Chatalic, K. L., Veldhoven-Zweistra, J., Bolkestein, M., Hoeben, S., Koning, G. A., Boerman, O. C., de Jong, M., & van Weerden, W. M. A Novel  $^{111}\text{In}$ -Labeled Anti-Prostate-Specific Membrane Antigen Nanobody for Targeted SPECT/CT Imaging of Prostate Cancer. *J. Nucl. Med. Off. Publ. Soc. Nucl. Med.* **56**, 1094–1099 (2015).
99. Lütje, S., van Rij, C. M., Franssen, G. M., Fracasso, G., Helfrich, W., Eek, A., Oyen, W. J., Colombatti, M., & Boerman, O. C. Targeting human prostate cancer with  $^{111}\text{In}$ -labeled D2B IgG, F(ab')<sub>2</sub> and Fab fragments in nude mice with PSMA-expressing xenografts. *Contrast Media Mol. Imaging* **10**, 28–36 (2015).
100. Parker, S. A., Diaz, I. L.-C., Anderson, K. A. & Batt, C. A. Design, production, and characterization of a single-chain variable fragment (ScFv) derived from the prostate specific membrane antigen (PSMA) monoclonal antibody J591. *Protein Expr. Purif.* **89**, 136–145 (2013).
101. Viola-Villegas, N. T., Sevak, K. K., Carlin, S. D., Doran, M. G., Evans, H. W., Bartlett, D. W., Wu, A. M., & Lewis, J. S. Noninvasive Imaging of PSMA in prostate tumors with (89)Zr-Labeled huJ591 engineered antibody fragments: the faster alternatives. *Mol. Pharm.* **11**, 3965–3973 (2014).



102. Pandit-Taskar, N., O'Donoghue, J. A., Ruan, S., Lyashchenko, S. K., Carrasquillo, J. A., Heller, G., Martinez, D. F., Cheal, S. M., Lewis, J. S., Fleisher, M., Keppler, J. S., Reiter, R. E., Wu, A. M., Weber, W. A., Scher, H. I., Larson, S. M., & Morris, M. J. First-in-Human Imaging with  $^{89}\text{Zr}$ -Df-IAB2M Anti-PSMA Minibody in Patients with Metastatic Prostate Cancer: Pharmacokinetics, Biodistribution, Dosimetry, and Lesion Uptake. *J. Nucl. Med.* **57**, 1858 (2016).
103. Cerchia, L., Giangrande, P. H., McNamara, J. O. & de Franciscis, V. Cell-specific aptamers for targeted therapies. *Methods Mol. Biol. Clifton NJ* **535**, 59–78 (2009).
104. Tuerk, C. & Gold, L. Systematic evolution of ligands by exponential enrichment: RNA ligands to bacteriophage T4 DNA polymerase. *Science* **249**, 505–510 (1990).
105. Sun, H. & Zu, Y. A Highlight of Recent Advances in Aptamer Technology and Its Application. *Mol. Basel Switz.* **20**, 11959–11980 (2015).
106. Zhuo, Z., Yu, Y., Wang, M., Li, J., Zhang, Z., Liu, J., Wu, X., Lu, A., Zhang, G., & Zhang, B. Recent Advances in SELEX Technology and Aptamer Applications in Biomedicine. *Int. J. Mol. Sci.* **18**, (2017).
107. Lupold, S. E., Hicke, B. J., Lin, Y. & Coffey, D. S. Identification and characterization of nuclease-stabilized RNA molecules that bind human prostate cancer cells via the prostate-specific membrane antigen. *Cancer Res.* **62**, 4029–4033 (2002).
108. Boyacioglu, O., Stuart, C. H., Kulik, G. & Gmeiner, W. H. Dimeric DNA Aptamer Complexes for High-capacity-targeted Drug Delivery Using pH-sensitive Covalent Linkages. *Mol. Ther. Nucleic Acids* **2**, e107 (2013).
109. Almasi, F., Mousavi Gargari, S. L., Bitaraf, F. & Rasoulinejad, S. Development of a Single Stranded DNA Aptamer as a Molecular Probe for LNCap Cells Using Cell-SELEX. *Avicenna J. Med. Biotechnol.* **8**, 104–111 (2016).

110. Atabi, F., Mousavi Gargari, S. L., Hashemi, M. & Yaghmaei, P. Doxorubicin Loaded DNA Aptamer Linked Myristilated Chitosan Nanogel for Targeted Drug Delivery to Prostate Cancer. *Iran. J. Pharm. Res. IJPR* **16**, 35–49 (2017).
111. Rockey, W. M., Huang, L., Kloepping, K. C., Baumhover, N. J., Giangrande, P. H., & Schultz, M. K. Synthesis and radiolabeling of chelator-RNA aptamer bioconjugates with copper-64 for targeted molecular imaging. *Bioorg. Med. Chem.* **19**, 4080–4090 (2011).
112. Kim, D., Jeong, Y. Y. & Jon, S. A Drug-Loaded Aptamer–Gold Nanoparticle Bioconjugate for Combined CT Imaging and Therapy of Prostate Cancer. *ACS Nano* **4**, 3689–3696 (2010).
113. Wang, A. Z., Bagalkot, V., Vasilliou, C. C., Gu, F., Alexis, F., Zhang, L., Shaikh, M., Yuet, K., Cima, M. J., Langer, R., Kantoff, P. W., Bander, N. H., Jon, S., & Farokhzad, O. C. Superparamagnetic iron oxide nanoparticle-aptamer bioconjugates for combined prostate cancer imaging and therapy. *ChemMedChem* **3**, 1311–1315 (2008).
114. Dassie, J. P., Hernandez, L. I., Thomas, G. S., Long, M. E., Rockey, W. M., Howell, C. A., Chen, Y., Hernandez, F. J., Liu, X. Y., Wilson, M. E., Allen, L. A., Vaena, D. A., Meyerholz, D. K., & Giangrande, P. H. Targeted inhibition of prostate cancer metastases with an RNA aptamer to prostate-specific membrane antigen. *Mol. Ther. J. Am. Soc. Gene Ther.* **22**, 1910–1922 (2014).
115. Chu, T. C., Twu, K. Y., Ellington, A. D. & Levy, M. Aptamer mediated siRNA delivery. *Nucleic Acids Res.* **34**, e73 (2006).
116. Zhen, S., Takahashi, Y., Narita, S., Yang, Y.-C. & Li, X. Targeted delivery of CRISPR/Cas9 to prostate cancer by modified gRNA using a flexible aptamer-cationic liposome. *Oncotarget* **8**, 9375–9387 (2017).

117. Kelly, L., Kratschmer, C., Maier, K. E., Yan, A. C. & Levy, M. Improved Synthesis and In Vitro Evaluation of an Aptamer Ribosomal Toxin Conjugate. *Nucleic Acid Ther.* **26**, 156–165 (2016).
118. Bagalkot, V., Farokhzad, O. C., Langer, R. & Jon, S. An aptamer-doxorubicin physical conjugate as a novel targeted drug-delivery platform. *Angew. Chem. Int. Ed Engl.* **45**, 8149–8152 (2006).
119. Farokhzad, O. C., Jon, S., Khademhosseini, A., Tran, T. N., Lavan, D. A., & Langer, R. Nanoparticle-aptamer bioconjugates: a new approach for targeting prostate cancer cells. *Cancer Res.* **64**, 7668–7672 (2004).
120. Pastor, F., Kolonias, D., McNamara, J. O. 2nd & Gilboa, E. Targeting 4-1BB costimulation to disseminated tumor lesions with bi-specific oligonucleotide aptamers. *Mol. Ther. J. Am. Soc. Gene Ther.* **19**, 1878–1886 (2011).
121. Zhou, J., Neale, J. H., Pomper, M. G. & Kozikowski, A. P. NAAG peptidase inhibitors and their potential for diagnosis and therapy. *Nat. Rev. Drug Discov.* **4**, 1015–1026 (2005).
122. Jackson, P. F., Cole, D. C., Slusher, B. S., Stetz, S. L., Ross, L. E., Donzanti, B. A., & Trainor, D. A. Design, synthesis, and biological activity of a potent inhibitor of the neuropeptidase N-acetylated alpha-linked acidic dipeptidase. *J. Med. Chem.* **39**, 619–622 (1996).
123. Jackson, P. F., Tays, K. L., Maclin, K. M., Ko, Y. S., Li, W., Vitharana, D., Tsukamoto, T., Stoermer, D., Lu, X. C., Wozniak, K., & Slusher, B. S. Design and pharmacological activity of phosphinic acid based NAALADase inhibitors. *J. Med. Chem.* **44**, 4170–4175 (2001).
124. Tang, H., Brown, M., Ye, Y., Huang, G., Zhang, Y., Wang, Y., Zhai, H., Chen, X., Shen, T. Y., & Tenniswood, M. Prostate targeting ligands based on N-acetylated alpha-linked acidic dipeptidase. *Biochem. Biophys. Res. Commun.* **307**, 8–14 (2003).

125. Jackson, P. F. & Slusher, B. S. Design of NAALADase inhibitors: a novel neuroprotective strategy. *Curr. Med. Chem.* **8**, 949–957 (2001).
126. Ding, P., Miller, M. J., Chen, Y., Helquist, P., Oliver, A. J., & Wiest, O. Syntheses of Conformationally Constricted Molecules as Potential NAALADase/PSMA Inhibitors. *Org. Lett.* **6**, 1805–1808 (2004).
127. Majer, P., Jančařík, A., Krečmerová, M., Tichý, T., Tenora, L., Wozniak, K., Wu, Y., Pommier, E., Ferraris, D., Rais, R., & Slusher, B. S. Discovery of Orally Available Prodrugs of the Glutamate Carboxypeptidase II (GCPII) Inhibitor 2-Phosphonomethylpentanedioic Acid (2-PMPA). *J. Med. Chem.* **59**, 2810–2819 (2016).
128. Liu, T., Toriyabe, Y., Kazak, M. & Berkman, C. E. Pseudoirreversible inhibition of prostate-specific membrane antigen by phosphoramidate peptidomimetics. *Biochemistry* **47**, 12658–12660 (2008).
129. Novakova, Z., Cerny, J., Choy, C. J., Nedrow, J. R., Choi, J. K., Lubkowski, J., Berkman, C. E., & Barinka, C. Design of composite inhibitors targeting glutamate carboxypeptidase II: the importance of effector functionalities. *FEBS J.* **283**, 130–143 (2016).
130. Majer, P., Jackson, P. F., Delahanty, G., Grella, B. S., Ko, Y. S., Li, W., Liu, Q., Maclin, K. M., Poláková, J., Shaffer, K. A., Stoermer, D., Vitharana, D., Wang, E. Y., Zakrzewski, A., Rojas, C., Slusher, B. S., Wozniak, K. M., Burak, E., Limsakun, T., & Tsukamoto, T. Synthesis and biological evaluation of thiol-based inhibitors of glutamate carboxypeptidase II: discovery of an orally active GCP II inhibitor. *J. Med. Chem.* **46**, 1989–1996 (2003).
131. van der Post, J. P., de Visser, S. J., de Kam, M. L., Woelfler, M., Hilt, D. C., Vornov, J., Burak, E. S., Bortey, E., Slusher, B. S., Limsakun, T., Cohen, A. F., & van Gerven, J. M. The central nervous system effects, pharmacokinetics and safety of the NAALADase-inhibitor GPI 5693. *Br. J. Clin. Pharmacol.* **60**, 128–136 (2005).

132. Majer, P., Hin, B., Stoermer, D., Adams, J., Xu, W., Duvall, B. R., Delahanty, G., Liu, Q., Stathis, M. J., Wozniak, K. M., Slusher, B. S., & Tsukamoto, T. Structural optimization of thiol-based inhibitors of glutamate carboxypeptidase II by modification of the P1' side chain. *J. Med. Chem.* **49**, 2876–2885 (2006).
133. Grella, B., Adams, J., Berry, J. F., Delahanty, G., Ferraris, D. V., Majer, P., Ni, C., Shukla, K., Shuler, S. A., Slusher, B. S., Stathis, M., & Tsukamoto, T. The discovery and structure–activity relationships of indole-based inhibitors of glutamate carboxypeptidase II. *Bioorg. Med. Chem. Lett.* **20**, 7222–7225 (2010).
134. Stoermer, D., Vitharana, D., Hin, N., Delahanty, G., Duvall, B., Ferraris, D. V., Grella, B. S., Hoover, R., Rojas, C., Shanholtz, M. K., Smith, K. P., Stathis, M., Wu, Y., Wozniak, K. M., Slusher, B. S., & Tsukamoto, T. Design, synthesis, and pharmacological evaluation of glutamate carboxypeptidase II (GCPII) inhibitors based on thioalkylbenzoic acid scaffolds. *J. Med. Chem.* **55**, 5922–32 (2012).
135. Blank, B. R., Alayoglu, P., Engen, W., Choi, J. K., Berkman, C. E., & Anderson, M. O. N-substituted glutamyl sulfonamides as inhibitors of glutamate carboxypeptidase II (GCP2). *Chem. Biol. Drug Des.* **77**, 241–247 (2011).
136. Choy, C. J., Fulton, M. D., Davis, A. L., Hopkins, M., Choi, J. K., Anderson, M. O., & Berkman, C. E. Rationally Designed Sulfamides as Glutamate Carboxypeptidase II Inhibitors. *Chem. Biol. Drug Des.* **82**, 612–619 (2013).
137. Kozikowski, A. P., Nan, F., Conti, P., Zhang, J., Ramadan, E., Bzdega, T., Wroblewska, B., Neale, J. H., Pshenichkin, S., & Wroblewski, J. T. Design of Remarkably Simple, Yet Potent Urea-Based Inhibitors of Glutamate Carboxypeptidase II (NAALADase). *J. Med. Chem.* **44**, 298–301 (2001).
138. Olszewski, R. T., Bukhari, N., Zhou, J., Kozikowski, A. P., Wroblewski, J. T., Shamimi-Noori, S., Wroblewska, B., Bzdega, T., Vicini, S., Barton, F. B., & Neale, J. H. NAAG

- peptidase inhibition reduces locomotor activity and some stereotypes in the PCP model of schizophrenia via group II mGluR. *J. Neurochem.* **89**, 876–885 (2004).
139. Yamamoto, T., Hirasawa, S., Wroblewska, B., Grajkowska, E., Zhou, J., Kozikowski, A., Wroblewski, J., & Neale, J. H. Antinociceptive effects of N-acetylaspartylglutamate (NAAG) peptidase inhibitors ZJ-11, ZJ-17 and ZJ-43 in the rat formalin test and in the rat neuropathic pain model. *Eur. J. Neurosci.* **20**, 483–494 (2004).
140. Chen, Y., Foss, C. A., Byun, Y., Nimmagadda, S., Pullambhatla, M., Fox, J. J., Castanares, M., Lupold, S. E., Babich, J. W., Mease, R. C., & Pomper, M. G. Radiohalogenated prostate-specific membrane antigen (PSMA)-based ureas as imaging agents for prostate cancer. *J. Med. Chem.* **51**, 7933–7943 (2008).
141. Kopka, K., Benešová, M., Bařinka, C., Haberkorn, U. & Babich, J. Glu-Ureido-Based Inhibitors of Prostate-Specific Membrane Antigen: Lessons Learned During the Development of a Novel Class of Low-Molecular-Weight Theranostic Radiotracers. *J. Nucl. Med. Off. Publ. Soc. Nucl. Med.* **58**, 17S-26S (2017).
142. Hofman, M. S., Violet, J., Hicks, R. J., Ferdinandus, J., Thang, S. P., Akhurst, T., Iravani, A., Kong, G., Ravi Kumar, A., Murphy, D. G., Eu, P., Jackson, P., Scalzo, M., Williams, S. G., & Sandhu, S. [(177)Lu]-PSMA-617 radionuclide treatment in patients with metastatic castration-resistant prostate cancer (LuPSMA trial): a single-centre, single-arm, phase 2 study. *Lancet Oncol.* **19**, 825–833 (2018).
143. Heck, M. M., Tauber, R., Schwaiger, S., Retz, M., D'Alessandria, C., Maurer, T., Gafita, A., Wester, H. J., Gschwend, J. E., Weber, W. A., Schwaiger, M., Knorr, K., & Eiber, M. Treatment Outcome, Toxicity, and Predictive Factors for Radioligand Therapy with 177Lu-PSMA-I&T in Metastatic Castration-resistant Prostate Cancer. *Eur. Urol.* **75**, 920–926 (2019).

144. Youn, S., Kim, K. I., Ptacek, J., Ok, K., Novakova, Z., Kim, Y., Koo, J., Barinka, C., & Byun, Y. Carborane-containing urea-based inhibitors of glutamate carboxypeptidase II: Synthesis and structural characterization. *Bioorg. Med. Chem. Lett.* **25**, 5232–5236 (2015).
145. Wang, S., Blaha, C., Santos, R., Huynh, T., Hayes, T. R., Beckford-Vera, D. R., Blecha, J. E., Hong, A. S., Fogarty, M., Hope, T. A., Raleigh, D. R., Wilson, D. M., Evans, M. J., VanBrocklin, H. F., Ozawa, T., & Flavell, R. R. Synthesis and Initial Biological Evaluation of Boron-Containing Prostate-Specific Membrane Antigen Ligands for Treatment of Prostate Cancer Using Boron Neutron Capture Therapy. *Mol. Pharm.* **16**, 3831–3841 (2019).
146. Barinka, C., Novakova, Z., Hin, N., Bím, D., Ferraris, D. V., Duvall, B., Kabarriti, G., Tsukamoto, R., Budesinsky, M., Motlova, L., Rojas, C., Slusher, B. S., Rokob, T. A., Rulíšek, L., & Tsukamoto, T. Structural and computational basis for potent inhibition of glutamate carboxypeptidase II by carbamate-based inhibitors. *Bioorg. Med. Chem.* **27**, 255–264 (2019).
147. Stoermer, D., Liu, Q., Hall, M. R., Flanary, J. M., Thomas, A. G., Rojas, C., Slusher, B. S., & Tsukamoto, T. Synthesis and biological evaluation of hydroxamate-Based inhibitors of glutamate carboxypeptidase II. *Bioorg. Med. Chem. Lett.* **13**, 2097–2100 (2003).
148. Novakova, Z., Wozniak, K., Jancarik, A., Rais, R., Wu, Y., Pavlicek, J., Ferraris, D., Havlinova, B., Ptacek, J., Vavra, J., Hin, N., Rojas, C., Majer, P., Slusher, B. S., Tsukamoto, T., & Barinka, C. Unprecedented Binding Mode of Hydroxamate-Based Inhibitors of Glutamate Carboxypeptidase II: Structural Characterization and Biological Activity. *J. Med. Chem.* **59**, 4539–4550 (2016).
149. Rais, R., Vávra, J., Tichý, T., Dash, R. P., Gadiano, A. J., Tenora, L., Monincová, L., Bařinka, C., Alt, J., Zimmermann, S. C., Slusher, C. E., Wu, Y., Wozniak, K., Majer, P., Tsukamoto, T., & Slusher, B. S. Discovery of a para-Acetoxy-benzyl Ester Prodrug of a

- Hydroxamate-Based Glutamate Carboxypeptidase II Inhibitor as Oral Therapy for Neuropathic Pain. *J. Med. Chem.* **60**, 7799–7809 (2017).
150. Davis, M. I., Bennett, M. J., Thomas, L. M. & Bjorkman, P. J. Crystal structure of prostate-specific membrane antigen, a tumor marker and peptidase. *Proc Natl Acad Sci U S A.* **102**, 5981- 5986 (2005).
151. Mesters, J. R., Barinka, C., Li, W., Tsukamoto, T., Majer, P., Slusher, B. S., Konvalinka, J., & Hilgenfeld, R. Structure of glutamate carboxypeptidase II, a drug target in neuronal damage and prostate cancer. *EMBO J.* **25**, 1375–1384 (2006).
152. Barinka, C., Starkova, J., Konvalinka, J. & Lubkowski, J. A high-resolution structure of ligand-free human glutamate carboxypeptidase II. *Acta Crystallograph. Sect. F Struct. Biol. Cryst. Commun.* **63**, 150–153 (2007).
153. Chevrier, B., Schalk, C., D'Orchymont, H., Rondeau, J. M., Moras, D., & Tarnus, C. Crystal structure of *Aeromonas proteolytica* aminopeptidase: a prototypical member of the co-catalytic zinc enzyme family. *Structure* **2**, 283–91 (1994).
154. Greenblatt, H. M., Almog, O., Maras, B., Spungin-Bialik, A., Barra, D., Blumberg, S., & Shoham, G. *Streptomyces griseus* aminopeptidase: X-ray crystallographic structure at 1.75 Å resolution. *J. Mol. Biol.* **265**, 620–636 (1997).
155. Barinka, C., Hlouchova, K., Rovenska, M., Majer, P., Dauter, M., Hin, N., Ko, Y. S., Tsukamoto, T., Slusher, B. S., Konvalinka, J., & Lubkowski, J. Structural Basis of Interactions between Human Glutamate Carboxypeptidase II and Its Substrate Analogs. *J. Mol. Biol.* **376**, 1438–1450 (2008).
156. Pinto, J. T., Suffoletto, B. P., Berzin, T. M., Qiao, C. H., Lin, S., Tong, W. P., May, F., Mukherjee, B., & Heston, W. D. Prostate-specific Membrane Antigen: A Novel Folate Hydrolase in Human Prostatic Carcinoma Cells. *Clinical Cancer Research* **2**, 1445–1451 (1996).



157. Pavlicek, J., Ptacek, J. & Barinka, C. Glutamate Carboxypeptidase II: An Overview of Structural Studies and Their Importance for Structure-Based Drug Design and Deciphering the Reaction Mechanism of the Enzyme. *Curr. Med. Chem.* **19**, 1300–1309 (2012).
158. Zhang, A. X., Murelli, R. P., Barinka, C., Michel, J., Cocleaza, A., Jorgensen, W. L., Lubkowski, J., & Spiegel, D. A. A Remote Arene-Binding Site on Prostate Specific Membrane Antigen Revealed by Antibody-Recruiting Small Molecules. *J. Am. Chem. Soc.* **132**, 12711–12716 (2010).
159. Ren, R., Mayer, B., Cicchetti, P. & Baltimore, D. Identification of a ten-amino acid proline-rich SH3 binding site. *Science* **259**, 1157–1161 (1993).
160. Yu, H., Chen, J. K., Feng, S., Dalgarno, D. C., Brauer, A. W., & Schreiber, S. L. Structural basis for the binding of proline-rich peptides to SH3 domains. *Cell* **76**, 933–945 (1994).
161. Barinka, C., Rojas, C., Slusher, B. & Pomper, M. Glutamate Carboxypeptidase II in Diagnosis and Treatment of Neurologic Disorders and Prostate Cancer. *Curr. Med. Chem.* **19**, 856–870 (2012).
162. Barinka, C., Rinnová, M., Sácha, P., Rojas, C., Majer, P., Slusher, B. S., & Konvalinka, J. Substrate specificity, inhibition and enzymological analysis of recombinant human glutamate carboxypeptidase II. *J. Neurochem.* **80**, 477–487 (2002).
163. Barinka, C., Byun, Y., Dusich, C. L., Banerjee, S. R., Chen, Y., Castanares, M., Kozikowski, A. P., Mease, R. C., Pomper, M. G., & Lubkowski, J. Interactions between Human Glutamate Carboxypeptidase II and Urea-Based Inhibitors: Structural Characterization. *J. Med. Chem.* **51**, 7737–7743 (2008).
164. Barinka, C., Rovenská, M., Mlcochová, P., Hlouchová, K., Plechanovová, A., Majer, P., Tsukamoto, T., Slusher, B. S., Konvalinka, J., & Lubkowski, J. Structural Insight into

- the Pharmacophore Pocket of Human Glutamate Carboxypeptidase II. *J. Med. Chem.* **50**, 3267–3273 (2007).
165. Ghosh, A. & Heston, W. D. W. Effect of carbohydrate moieties on the folate hydrolysis activity of the prostate specific membrane antigen. *The Prostate* **57**, 140–151 (2003).
166. Holmes, E. H., Greene, T. G., Tino, W. T., Boynton, A. L., Aldape, H. C., Misrock, S. L., & Murphy, G. P. Analysis of glycosylation of prostate-specific membrane antigen derived from LNCaP cells, prostatic carcinoma tumors, and serum from prostate cancer patients. *The Prostate* **7**, 25–29 (1996)
167. Barinka, C., Sácha, P., Sklenár, J., Man, P., Bezouska, K., Slusher, B. S., & Konvalinka, J. Identification of the N-glycosylation sites on glutamate carboxypeptidase II necessary for proteolytic activity. *Protein Sci.* **13**, 1627-1635 (2004).
168. Schülke, N., Varlamova, O. A., Donovan, G. P., Ma, D., Gardner, J. P., Morrissey, D. M., Arrigale, R. R., Zhan, C., Chodera, A. J., Surowitz, K. G., Maddon, P. J., Heston, W. D., & Olson, W. C. The homodimer of prostate-specific membrane antigen is a functional target for cancer therapy. *Proc. Natl. Acad. Sci.* **100**, 12590–12595 (2003).
169. Ptacek, J., Nedvedova, J., Navratil, M., Havlinova, B., Konvalinka, J., & Barinka, C. The calcium-binding site of human glutamate carboxypeptidase II is critical for dimerization, thermal stability, and enzymatic activity: Calcium is Required for GCPII Function. *Protein Sci.* **27**, 1575–1584 (2018).
170. Klusák, V., Barinka, C., Plechanovová, A., Mlcochová, P., Konvalinka, J., Rulísek, L., & Lubkowski, J. Reaction Mechanism of Glutamate Carboxypeptidase II Revealed by Mutagenesis, X-ray Crystallography, and Computational Methods. *Biochemistry* **48**, 4126–4138 (2009).

171. Chen, S.-L., Marino, T., Fang, W.-H., Russo, N. & Himo, F. Peptide Hydrolysis by the Binuclear Zinc Enzyme Aminopeptidase from *Aeromonas proteolytica*: A Density Functional Theory Study. *J. Phys. Chem. B* **112**, 2494–2500 (2008).
172. Gilboa, R., Spungin-Bialik, A., Wohlfahrt, G., Schomburg, D., Blumberg, S., & Shoham, G. Interactions of *Streptomyces griseus* aminopeptidase with amino acid reaction products and their implications toward a catalytic mechanism. *Proteins Struct. Funct. Genet.* **44**, 490–504 (2001).
173. Hlouchová, K., Barinka, C., Klusák, V., Sácha, P., Mlcochová, P., Majer, P., Rulísek, L., & Konvalinka, J. Biochemical characterization of human glutamate carboxypeptidase III. *J. Neurochem.* **101**, 682–696 (2007).
174. Tiffany, C. W. & Slusher, B. S. Measurement of Glutamate Carboxypeptidase II (NAALADase) Enzyme Activity by the Hydrolysis of [<sup>3</sup>H]-*N*-Acetylaspartylglutamate (NAAG). *Curr Protoc Pharmacol.* Chapter 3:Unit3.10 (2002)
175. Rojas, C., Frazier, S. T., Flanary, J. & Slusher, B. S. Kinetics and inhibition of glutamate carboxypeptidase II using a microplate assay. *Anal. Biochem.* **310**, 50–54 (2002).
176. Roth, Marc. Fluorescence reaction for amino acids. *Anal. Chem.* **43**, 880–882 (1971).
177. Simons, S. S. & Johnson, D. F. Reaction of o-phthalaldehyde and thiols with primary amines: Fluorescence properties of 1-alkyl(and aryl)thio-2-alkylisoindoles. *Anal. Biochem.* **90**, 705–725 (1978).
178. Anderson, M. O., Wu, L. Y., Santiago, N. M., Moser, J. M., Rowley, J. A., Bolstad, E. S., & Berkman, C. E. Substrate specificity of prostate-specific membrane antigen. *Bioorg. Med. Chem.* **15**, 6678–6686 (2007).
179. Maung, J., Mallari, J. P., Girtsman, T. A., Wu, L. Y., Rowley, J. A., Santiago, N. M., Brunelle, A. N., & Berkman, C. E. Probing for a hydrophobic a binding register in prostate-

- specific membrane antigen with phenylalkylphosphonamidates. *Bioorg. Med. Chem.* **12**, 4969–4979 (2004).
180. Plechanovová, A., Byun, Y., Alquicer, G., Skultétyová, L., Mlčochová, P., Němcová, A., Kim, H. J., Navrátil, M., Mease, R., Lubkowski, J., Pomper, M., Konvalinka, J., Rulišek, L., & Bařinka, C. Novel Substrate-Based Inhibitors of Human Glutamate Carboxypeptidase II with Enhanced Lipophilicity. *J. Med. Chem.* **54**, 7535–7546 (2011).
181. Alquicer, G., Sedlák, D., Byun, Y., Pavlíček, J., Stathis, M., Rojas, C., Slusher, B., Pomper, M. G., Bartunek, P., & Barinka, C. Development of a High-Throughput Fluorescence Polarization Assay to Identify Novel Ligands of Glutamate Carboxypeptidase II. *J. Biomol. Screen.* **17**, 1030–1040 (2012).
182. Amplex® Red Glutamic Acid/Glutamate Oxidase Assay Kit Protocol.
183. Zhou, M., Diwu, Z., Panchuk-Voloshina, N. & Haugland, R. P. A stable nonfluorescent derivative of resorufin for the fluorometric determination of trace hydrogen peroxide: applications in detecting the activity of phagocyte NADPH oxidase and other oxidases. *Anal. Biochem.* **253**, 162–168 (1997).
184. Mohanty, J. G., Jaffe, J. S., Schulman, E. S. & Raible, D. G. A highly sensitive fluorescent micro-assay of H<sub>2</sub>O<sub>2</sub> release from activated human leukocytes using a dihydroxyphenoxazine derivative. *J. Immunol. Methods* **202**, 133–141 (1997).
185. Kawatani, M., Yamamoto, K., Yamada, D., Kamiya, M., Miyakawa, J., Miyama, Y., Kojima, R., Morikawa, T., Kume, H., & Urano, Y. Fluorescence Detection of Prostate Cancer by an Activatable Fluorescence Probe for PSMA Carboxypeptidase Activity. *J. Am. Chem. Soc.* **141**, 10409–10416 (2019).
186. Murshudov, G. N., Skubák, P., Lebedev, A. A., Pannu, N. S., Steiner, R. A., Nicholls, R. A., Winn, M. D., Long, F., & Vagin, A. A. REFMAC5 for the refinement of macromolecular crystal structures. *Acta Crystallogr. Sect. D* **67**, 355–367 (2011).

187. Emsley, P. & Cowtan, K. Coot: model-building tools for molecular graphics. *Acta Crystallogr. Sect. D* **60**, 2126–2132 (2004).
188. Long, F., Nicholls, R. A., Emsley, P., Graáulis, S., Merkys, A., Vaitkus, A., & Murshudov, G. N. AceDRG: a stereochemical description generator for ligands. *Acta Crystallogr. Sect. Struct. Biol.* **73**, 112–122 (2017).
189. Chen, V. B., Arendall, W. B., 3rd, Headd, J. J., Keedy, D. A., Immormino, R. M., Kapral, G. J., Murray, L. W., Richardson, J. S., & Richardson, D. C. MolProbity: all-atom structure validation for macromolecular crystallography. *Acta Crystallogr. D Biol. Crystallogr.* **66**, 12–21 (2010).
190. Goldberg, J. M., Batjargal, S., Chen, B. S. & Petersson, E. J. Thioamide Quenching of Fluorescent Probes through Photoinduced Electron Transfer: Mechanistic Studies and Applications. *J. Am. Chem. Soc.* **135**, 18651–18658 (2013).
191. Goldberg, J. M., Speight, L. C., Fegley, M. W. & Petersson, E. J. Minimalist probes for studying protein dynamics: thioamide quenching of selectively excitable fluorescent amino acids. *J. Am. Chem. Soc.* **134**, 6088–6091 (2012).
192. Goldberg, J. M., Wissner, R. F., Klein, A. M. & Petersson, E. J. Thioamide quenching of intrinsic protein fluorescence. *Chem Commun* **48**, 1550–1552 (2012).
193. Goldberg, J. M., Chen, X., Meinhardt, N., Greenbaum, D. C. & Petersson, E. J. Thioamide-based fluorescent protease sensors. *J. Am. Chem. Soc.* **136**, 2086–2093 (2014).